Experimental Investigation of Nano-Fluid Characteristics and Behavior of
Aluminum Oxide Nano-Particles Dispersed in Ethylene Glycol-Water Mixture

by

Jinghai Xu

A dissertation submitted in partial fulfillment
of the requirements for the degree of
Doctor of Philosophy
(Automotive Systems Engineering)
in the University of Michigan-Dearborn
2016

Doctoral Committee:

      Associate Professor Krisanu Bandyopadhyay, Co-Chair
      Associate Professor Dohoy Jung, Co-Chair
      Professor John Cherng
      Associate Professor Eric B. Ratts

TABLE OF CONTENTS

LIST OF FIGURES

LIST OF TABLES

NOMENCLATURE

A_i : inside surface area

a : diameter ratio, $D_{i,o}/D_{o,i}$

C_p : specific heat

D : diameter

D_h : hydraulic diameter

$D_{h,a}$: hydraulic diameter of annulus

$D_{i,i}$: inner diameter of inside tube

$D_{o,i}$: outer diameter of inside tube

$D_{i,o}$: inner diameter of outside tube

f : friction factor

h : convection coefficient

k : thermal conductivity

L : tube length

$\dot{m}$: mass flow rate

Nu : Nusselt number

Pr : Prandtl number

q : heat transfer rate

R : thermal resistance

$r_{i,i}$	: inside tube inner radius
$r_{o,i}$	: inside tube outer radius
Re	: Reynolds number
T	: temperature
T_1	: inner surface temperature of inside tube
T_2	: outer surface temperature of inside tube
ΔT_{lm}	: log mean temperature difference
U	: overall heat transfer coefficient
V	: average flow velocity

Greek

ϕ	: volume fraction
ρ	: density
μ	: dynamic viscosity

Subscripts

bf	: base fluid
c	: cooling fluid
$conv$	: convection heat transfer
cyl	: conduction heat transfer (cylinder wall)
exp	: experimental
h	: heating fluid
i	: inside fluid

inlet	: tube inlet
nf	: nano-fluid
o	: outside fluid
outlet	: tube outlet
p	: nano-particle
w	: tube wall

Abbreviation

ADC	: analog to digital converter
DLS	: dynamic light scattering
DW	: distilled water
EG	: ethylene glycol
ELS	: electrophoretic light scattering
EMF	: electromotive force
TEM	: transmission electron microscopy
UV-Vis	: ultraviolet-visible
50/50 EG/DW	: 50/50 vol.% ethylene glycol/water mixture

ABSTRACT

The need for improved efficiency of automotive thermal management system is
driven by the trend that the automotive powertrain system operates towards higher power
output with smaller system size. In other words, the intensified heat dissipation loads
from the powertrain system need more efficient cooling solutions. One effort is to
enhance the thermal performance of the conventional automotive heat transfer fluid,
typically ethylene glycol/water mixture, due to its intrinsically poor thermal property.
Nano-fluids have been synonymous with the nanotechnology-based advanced cooling
fluids which are derived by homogeneously dispersing nanometer-sized particles into
conventional heat transfer fluids.

In this study, a multi-parameter approach is used to investigate the behavior of the
Aluminum Oxide (Al_2O_3) nano-particle based nano-fluids. The nano-particles are
dispersed in 50/50 vol.% ethylene glycol/distilled water mixture and the other two base
fluids (distilled water and ethylene glycol). Two-step method is used for the nano-fluid
sample preparation. Nano-fluid sample is characterized by TEM imaging, particle surface
charge, particle sizing, light absorbance and pH. Nano-fluid thermal properties are
investigated by measuring the thermal conductivity and viscosity at different
temperatures. The nano-particle sedimentation within the nano-fluid is determined. The
aging effect on the nano-fluid thermal properties is studied. The results offer multiple-
perspective correlations between the nano-fluid characterization and performance.

Further, the experimental investigation is conducted to evaluate the forced convection heat transfer coefficient of Al_2O_3 based nano-fluids in the Reynolds number range of 3000 to 4000. The different nano-particle concentrations are tested. The heat transfer test section is basically a concentric double pipe heat exchanger. The inside pipe is designed to simulate a vehicle radiator tube flow condition, where the heated nano-fluid is circulating. The outside pipe is used for circulating the cooling water. The nano-fluid temperature at the inlet of the test section is kept at 60°C ±5°C. The result develops the correlation between nano-fluid convection heat transfer coefficient and Reynolds number as a function of nano-particle concentration.

CHAPTER I

Introduction

The need for improved efficiency of automotive thermal management system is driven by the trend that the automotive powertrain system operates towards higher power output with smaller system size. In other words, the intensified heat dissipation loads from the powertrain system need more efficient cooling solutions. One effort is to enhance the thermal performance of the conventional automotive heat transfer fluid, typically ethylene glycol/water mixture, due to its intrinsically poor thermal property. Inspired by the Maxwell's study [1] of the effective thermal conductivity of suspensions that contain solid particles, nano-fluids have been synonymous with the nanotechnology-based advanced cooling fluids which are derived by homogeneously dispersing nanometer-sized particles into conventional heat transfer fluids. Nano-fluids have been reported by many studies [2-7] providing unprecedented thermal performance improvement compared to conventional fluids.

Al_2O_3 is one of the most common nano-particle materials used in nano-fluid for enhanced heat transfer. There are several reasons for Al_2O_3 nano-particle being widely used in nano-fluid studies. Lower cost of the Al_2O_3 enables its mass production and makes it broadly commercially available [8]. Al_2O_3 nano-particle is categorized as a ceramic nano-particle [9] which, unlike many metallic nano-particles, is not susceptible to surface oxidation and is much easier to incorporate into a fluid [10]. Although the

thermal conductivity of Al_2O_3 is not significantly high among the other metal oxide materials such as CuO and ZnO, it is two orders of magnitude higher than those of the conventional heat transfer fluids [11].

The research studies of nano-fluid are usually categorized into two categories: nano-fluid property study and nano-fluid heat transfer performance study. The property studies mainly focus on examining the indicators of improved thermo-physical performance such as effective thermal conductivity and viscosity. The heat transfer performance studies evaluate the heat transfer performance through measuring the convection heat transfer coefficient.

Review papers [12-16] show that extensive property study research has been conducted on the Al_2O_3 nano-particle dispersed in base fluids of water and ethylene glycol. However, there are limited studies on the ethylene glycol and water mixture based Al_2O_3 nano-fluids. Vajjha *et al*. [17] investigated the thermal conductivity of Al_2O_3 nano-particle dispersed in 60/40 wt.% ethylene glycol/water. The particle volume fraction was tested up to 10% over the temperature range of 16.85°C to 89.85°C. Their result showed that the thermal conductivity of the nano-fluid over the base fluid increased with the increase in particle concentration and temperature. The nano-particle size effect was also studied and it was found that thermal conductivity decreased with increased particle diameter. Beck *et al*. [18] measured the thermal conductivity of 50/50 wt.% ethylene glycol/water based Al_2O_3 nano-fluids over an extended temperature range (up to 146.85°C). The volume fraction tested was from 0.5% to 4%. Al_2O_3 nano-particles of two particle sizes (10 and 50 nm) were tested in their study. They claimed that the thermal conductivity-temperature behavior of the nano-fluid followed closely the behavior of

base fluid. The thermal conductivity enhancement of the 10 nm particle was smaller than that of the 50 nm particle. LotfizadehDehkordi et al. [19] studied the viscosity of 0.01-1 vol.% Al_2O_3 nano-particle dispersed in 60/40 wt.% ethylene glycol/water with the addition of dispersant over the temperature range of 25-40°C. The increase in nano-fluid viscosity showed a nonlinear relationship with the particle loading. The nano-fluid viscosity was found to be highly temperature dependent. Yiamsawas et al. [20] investigated the viscosity of Al_2O_3 nano-particle suspended in a mixture of ethylene glycol/water (20/80 wt.%). The experiments were conducted at volume fractions from 0% to 4% and the temperature range of 15-60°C. The results indicated that the nano-fluid viscosity increased when particle loading increased and temperature decreased. The differences among the viscosities of nano-fluids at various particle loadings decreased with the increase in temperature. In Syam Sundar et al.'s study [21], Al_2O_3 nano-particles were dispersed in different ethylene glycol/water mixtures (20/80 wt.%, 40/60 wt.% and 60/40 wt.%). The thermal conductivity and viscosity were measured for the temperature range of 20-60°C and the particle volume concentrations from 0.3% to 1.5%. They found that the enhancements of nano-fluid in thermal conductivity and the viscosity depended not only on the particle concentration and temperature but also on the base fluid properties.

These experiments mainly focused on the nano-fluid property study. Some of them showed the correlation between nano-fluid characteristics and properties. However, since the number of nano-fluid characteristic parameters studied was limited, they did not provide a systematic view on the mechanism behind the nano-fluid properties. Nano-fluids are multivariable systems, with each thermo-physical property depending on

several parameters including nano-particle material, concentration, size and shape, properties of the base fluid, presence of additives, surfactants, electrolyte strength, and pH [22]. Therefore, a multi-parameter approach is used to investigate the behavior of the Al_2O_3 nano-particle based nano-fluids in this study. The nano-particles are dispersed in 50/50 vol.% ethylene glycol/distilled water mixture and the other two base fluids (distilled water and ethylene glycol). Two-step method is used for the nano-fluid sample preparation. Nano-fluid sample is characterized by TEM imaging, particle surface charge, particle sizing, light absorbance and pH. Nano-fluid thermal properties are investigated by measuring the thermal conductivity and viscosity at different temperatures. The nano-particle sedimentation within the nano-fluid is determined. The aging effect on the nano-fluid thermal properties is studied. The results are expected to offer multiple-perspective correlations between the nano-fluid characterization and performance.

The heat transfer performance of Al_2O_3 nano-particle based ethylene glycol and water mixture was rarely studied. Jung *et al*. [23] measured the convective heat transfer coefficient of a Al_2O_3 nano-particle based 50/50% water and ethylene glycol mixture in the laminar flow regime. The nano-fluid was pumped through the micro-channel for cooling the test chip. They claimed the Nusselt number did not vary dramatically with the nano-particle volume fraction over the tested Reynolds number range. Kulkarni *et al*. [24] evaluated the cogeneration and heat exchanger efficiency of a diesel electric generator with nano-fluid as the coolant. The nano-fluid coolant was Al_2O_3 nano-particles dispersed in 50/50 inhibited ethylene glycol and water mixture. While the investigation showed that the application of nano-fluid resulted in a reduction of cogeneration efficiency, the efficiency of heat exchanger increased. The efficiency increased from 78.1% of ethylene

glycol-water mixture to 81.11% for 6 vol.% Al_2O_3 nano-fluid. Vajjha *et al*. [25] numerically studied the heat transfer performance of Al_2O_3 in the 60/40 wt.% ethylene glycol and water mixture circulating through the flat tubes of an automotive radiator. The numerical computations were carried out in the complete laminar regime with the Reynolds number ranging from 100 to 2000. The result showed the Al_2O_3 nano-fluids with various particle volumetric concentrations exhibited substantial increase in the average heat transfer coefficient over the entire tube. A 10 vol.% Al_2O_3 nano-fluid had a 94% increase in the average heat transfer coefficient over the base fluid at the Reynolds number of 2000. Peyghambarzadeh *et al*. [26] measured Nusselt numbers of Al_2O_3 based nano-fluids. Different concentrations of ethylene glycol and water mixtures, which contained 5, 10 and 20 vol.% ethylene glycol, were used as the base fluids. The nano-fluid was circulated through a car radiator in order to perform forced convection heat transfer. The nano-fluid inlet temperature to the radiator was kept constantly at 45°C. They proved that the addition of nano-particle to each base fluid enhances the heat transfer coefficient. Yu *et al*. [27] measured the convective heat transfer coefficient of Al_2O_3 nano-particles dispersed in the 45/55 vol.% ethylene glycol and water mixture in the laminar flow regime. The nano-fluids were heated to 60°C in a heating bath, and then flowed into a −15°C cooling bath, where the heat transfer coefficient was measured. At the Reynolds number of 2000, the convective coefficients of nano-fluids with 1 vol.% and 2 vol.% nano-particle increased by 57% and 106% respectively over the base fluid. Selvakumar *et al*. [28] studied the effect of a 0.1 vol.% Al_2O_3 nano-particle based 30/70 vol.% ethylene glycol and water mixture nano-fluid in heat transfer and pressure drop in a rectangular channel copper heat sink. The convective heat transfer coefficients were

5

measured over the flow rate range of 0.207-0.563 GPM. The rise in convective heat transfer coefficient of Al_2O_3 nano-fluid is 11.94% compared to the plain ethylene glycol and water mixture. The pressure drop associated with the nano-fluid in the heat sink is around 5% higher than that of the base fluid, which was considered to be a not significant rise in pressure drop. Zhu *et al*. [29] studied the laminar convection heat transfer in a wavy channel of a Al_2O_3 nano-particle based 60/40 wt.% ethylene glycol and water mixture using computational fluid dynamics (CFD) simulation. The simulations were conducted in the Reynolds number range of 400 to 1200. The results showed the application of nano-fluid could provide efficient heat transfer capability, while the pressure drop increase due to the augmentation in fluid viscosity could not be neglected. They proposed an optimal range of Reynolds number and nano-particle concentration where the performance of nano-fluid could be beneficial.

In this study, the experimental investigation is conducted to evaluate the forced convection heat transfer coefficient of Al_2O_3 based nano-fluids in the Reynolds number range of 3000 to 4000. The base fluid is the 50/50 vol.% ethylene glycol/distilled water mixture. The different nano-particle concentrations are tested. The heat transfer test section is basically a concentric double pipe heat exchanger. The inside pipe is designed to simulate a vehicle radiator tube flow condition, where the heated nano-fluid is circulating. The outside pipe is used for circulating the cooling water. The nano-fluid temperature at the inlet of the test section is kept at 60°C ±5°C. The result is expected to provide data for developing the correlation between nano-fluid convection heat transfer coefficient and Reynolds number as a function of nano-particle concentration.

CHAPTER II

Experimental Setup

2.1 Nano-fluid Material and Characterization

2.1.1 Material

Al_2O_3 nano-particle used in this study was purchased from Nanophase

Technologies Corporation (Romeoville, IL, USA). The particles are claimed to be

spherical with a mean particle size of 40 nm by the manufacturer.

Distilled water (DW) was used as one of the base fluids. Pure ethylene glycol

(EG) was purchased from Alfa Aesar (99%, Product No. A11591). The 50/50 vol.%

ethylene glycol/water mixture (50/50 EG/DW) was made by mixing the distilled water

with pure ethylene glycol.

2.1.2 Transmission Electron Microscopy

Transmission electron microscopy (TEM) is one of the most common device used

for characterize the nano-particle. TEM images obtained from the TEM device (Hitachi

High Technologies America, Inc., Model HT7700) confirmed the particle sphericity, as

shown in Figure 1. However, the mean particle size was found to be 29.7 nm with a

standard deviation of 15.0 nm based on the number-weighted particle size analysis. The

particle size ranges from under 10 nm to 80 nm, as shown in Figure 2.
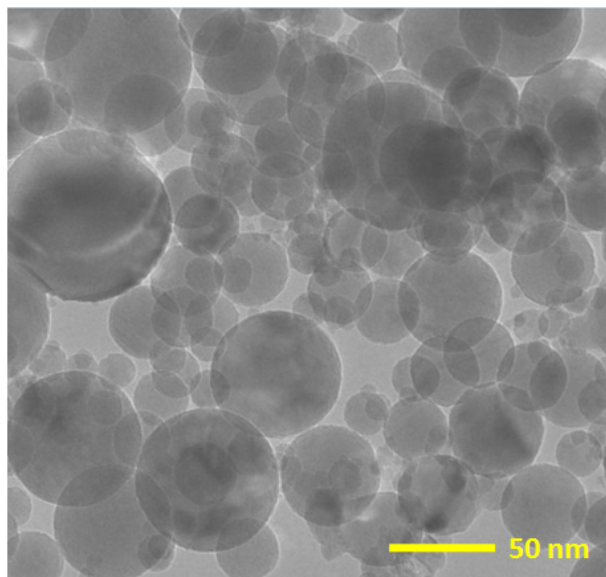
Figure 1. TEM image of Al_2O_3 nano-particles
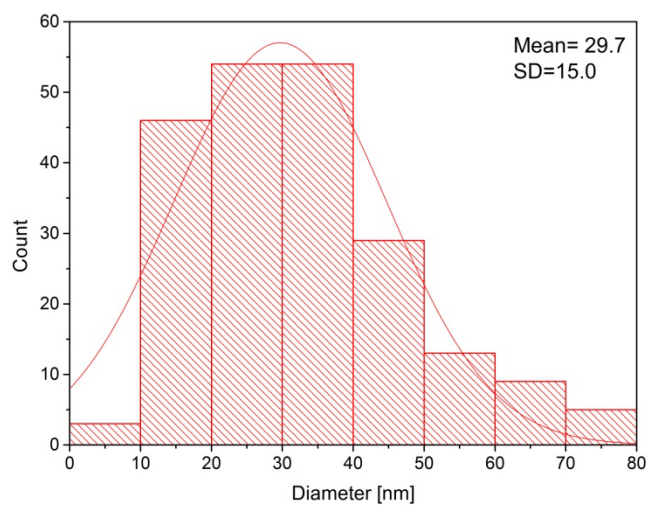
Figure 2. Histogram of Al_2O_3 nano-particle diameter

2.1.3 Nano-particle Surface Charge

Particle surface charge (zeta potential) was measured with a particle analyzer (Beckman Coulter, Inc., Model Delsa Nano C), which employed Electrophoretic Light Scattering (ELS) technique. Zeta potential is the potential at a position close to the boundary between the Stern layer and the Diffuse layer, as shown in Figure 3.
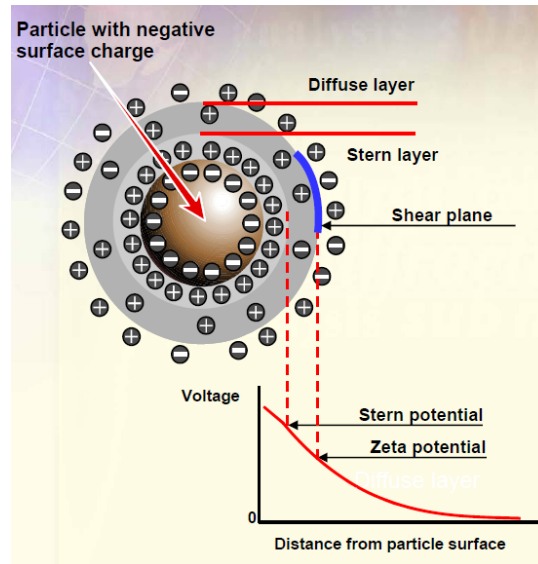
Figure 3. Zeta potential [30]

When measuring the zeta potential, the particle analyzer device uses a laser beam to irradiate the particles and detects the scattering light emitted from the particles. The scattered light from the moving particles is mixed with a reference beam. When there is no electric field applied to the sample cell, the scattered light and reference beam will have the same frequency, as shown in Figure 4(a). When an electrical field is applied, the frequency of scattered light is shifted from the frequency of the reference beam due to particles motion, as shown in Figure 4(b). This frequency shift of the scattering light is proportional to the speed of the particles movement [30]. The mobility of the particles can be measured from the frequency shift of the scattering light. Once the mobility of the particle is determined, the zeta potential of the particle can be derived.
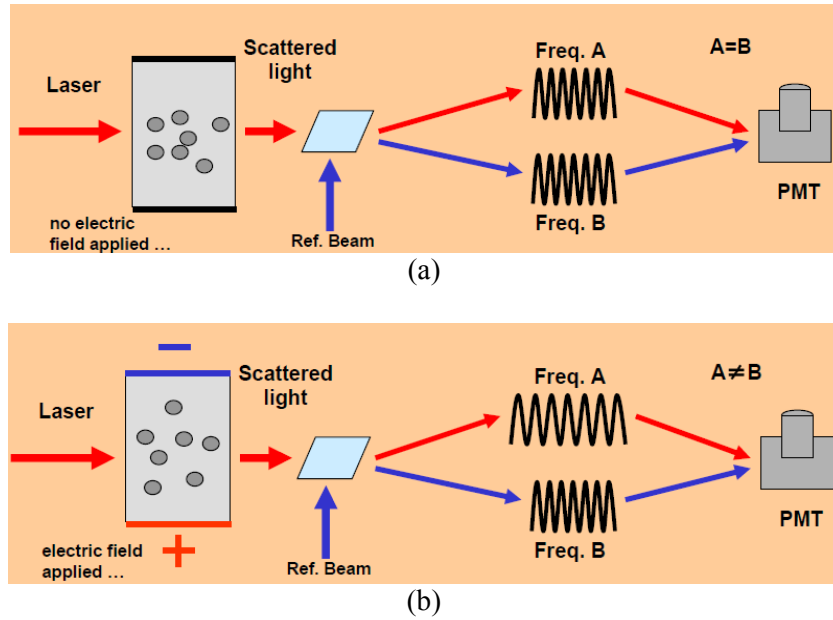
Figure 4. Operation theory of zeta potential measurement [30]

The absolute value of the particle zeta potential is an indicator of the strength of the repulsive force between the particles. The sufficient repulsive force can counteract the natural attractive force between the particles to prevent particles from aggregation. Otherwise, particles tend to aggregate. The zeta potentials of 0.1 g Al_2O_3 nano-particles in 10 mL of 3 base fluids (DW, EG and 50/50 EG/DW) were measured. Each sample was prepared by mixing the nano-powder with base fluid for 1 minute using a vortex mixer (Thermo Fisher Scientific, Inc.) prior to measuring.

2.1.4 Nano-particle Size

The dispersed particle aggregate size was measured by a particle analyzer (Beckman Coulter, Inc., Model Delsa Nano C) based on the Dynamic Light Scattering (DLS) technique.

Particles suspended in liquids are in Brownian motion because of the particles random collisions with solvent molecules. Brownian motion also causes the particles to diffuse through the medium. The diffusion coefficient D is inversely proportional to the particle size according to the Stokes-Einstein equation [30]:

$$D = \frac{k_B T}{3\pi\eta_0 d}$$

where, k_B is Boltzmann's constant, T is absolute temperature, η_0 is viscosity, d is hydrodynamic diameter. This equation indicates for large particles, D will be relatively small and the particles will move slowly. While for smaller particles, D will be larger and the particles will move rapidly. In dynamic light scattering, the fluctuations in time of scattered light from particles in Brownian motion are measured [30]. Figure 5 shows how particle size is determined by the dynamic light scattering method. For smaller, faster moving particles, the fluctuations will occur rapidly. For larger, slower moving particles, it will occur more slowly. The fluctuations of the scattered light are further analyzed by an autocorrelation function. For small particles with rapid motion and rapid intensity fluctuations, the autocorrelation function is a rapidly decaying exponential function with a large decay constant, while for large particles the exponential decays more slowly with a smaller decay constant [30]. For monodisperse particles, the logarithm of the autocorrelation function will become a straight line. For polydisperse samples, the logarithm of the autocorrelation function will exhibit a curvature line. The particle diameter is calculated from the decay constant. The particle size distributions are resolved from the measured autocorrelation functions.
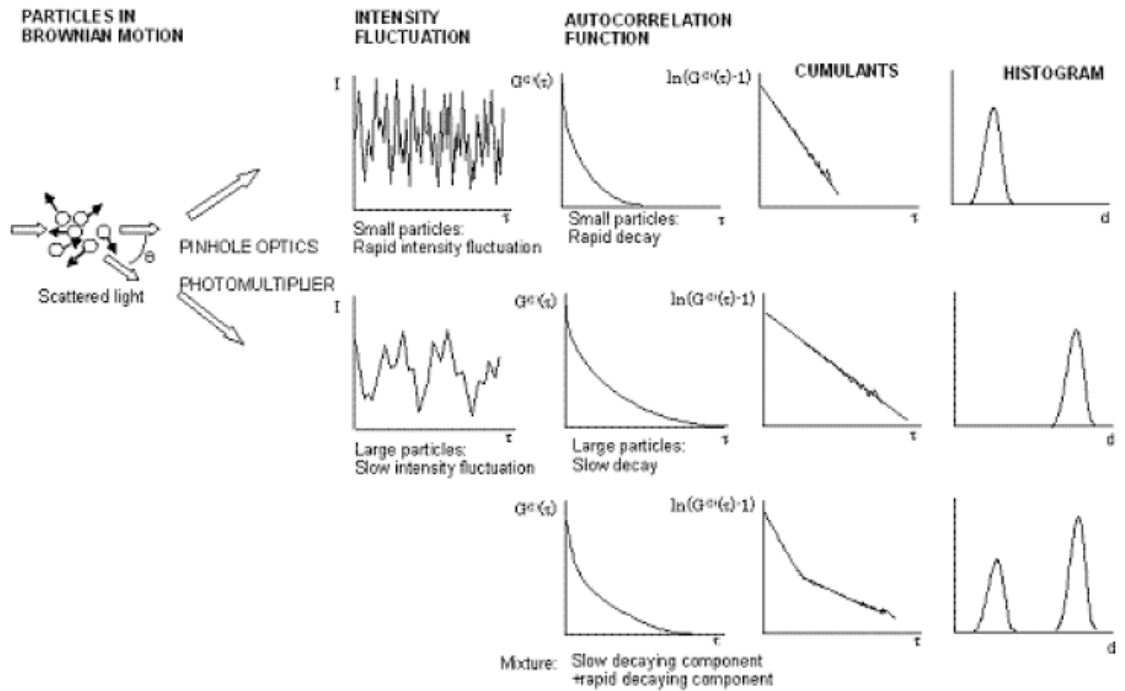
Figure 5. Determination of particle size by dynamic light scattering [30]

2.1.5 Nano-fluid Light Absorbance

According to the Beer's law [31], the particle concentration in the nano-fluid directly affects the light absorbance of nano-fluid. A light absorbance test procedure was developed for the particle sedimentation study as shown in Figure 6.
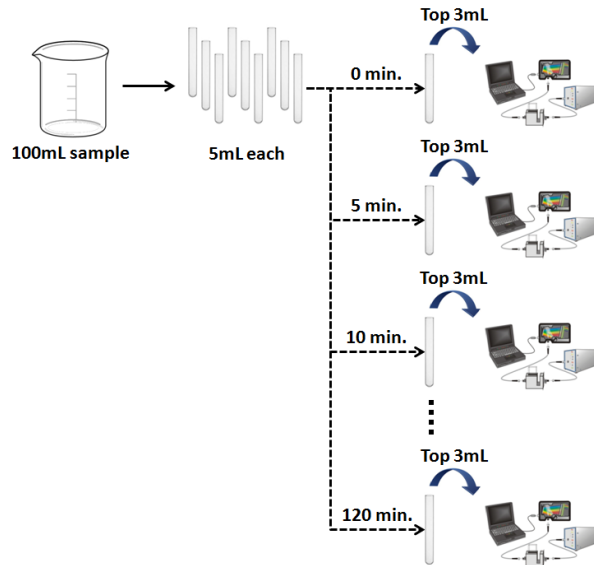
Figure 6. Light absorbance experiment procedure for particle sedimentation study

According to the procedure, the supernatant concentration of nano-fluid sample was measured with an ultraviolet-visible (UV-Vis) spectrometer (Ocean Optics, Inc., Model USB4000) in 5 minutes intervals for the first 30 minutes and in 15 minute intervals for the rest 90 minutes. First of all, a 100 mL fresh sample was distributed into twenty 13×100 mm borosilicate glass culture tubes with 5 mL in each tube, as shown in Figure 7. Then, the tubes were kept undisturbed. The first light absorbance spectrum was obtained right after the distribution, by taking a 3 mL sample using a pipette from the very top of one of the 5 mL sample tubes and loaded into the cuvette of the light absorbance test assembly for scanning. Then, the first spectrum represented the absorbance of sample without particle sedimentation. After 5 minutes, another 3 mL sample was taken from another 5 mL sample tube and loaded into the cuvette. The light absorbance was measured again. The light absorbance measurement was repeated in the predetermined time interval until the total experiment time reached 120 minutes. Eventually, the light absorbance spectra comprised of the single spectrum measured at

the specific time was obtained as a function of wavelength, as shown in Figure 8, for 5 wt.% Al_2O_3 in three different base fluids.
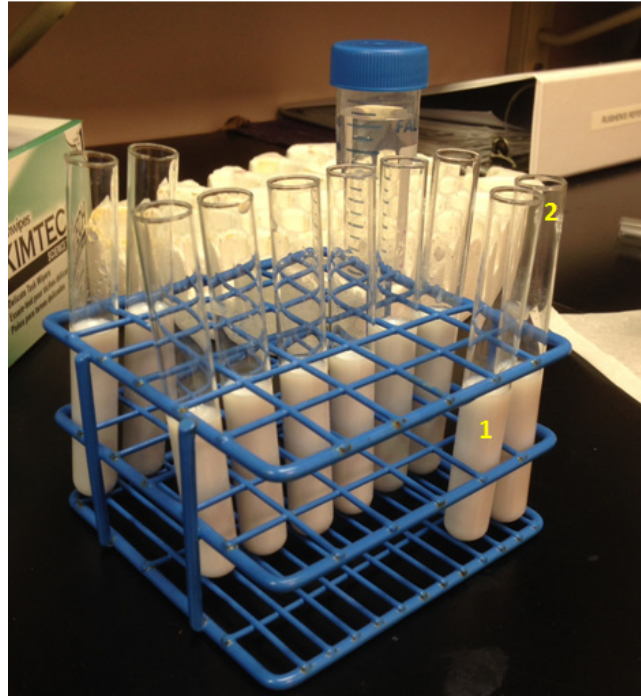
Figure 7. Nano-fluid sample set for light absorbance study
1. nano-fluid sample, 2. culture tube
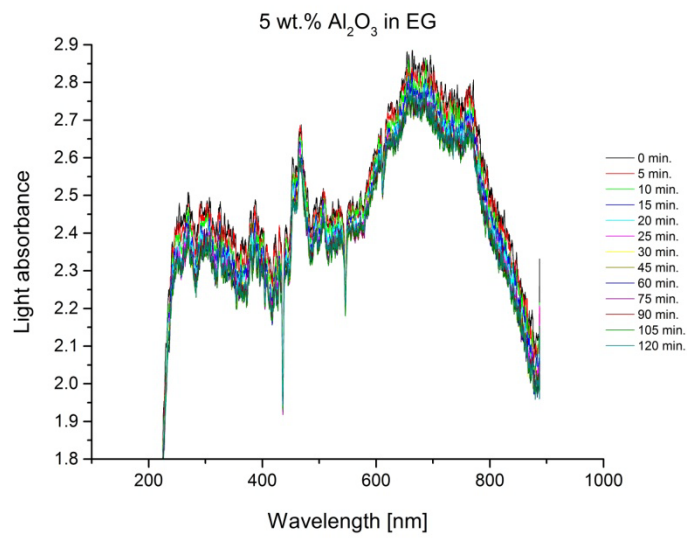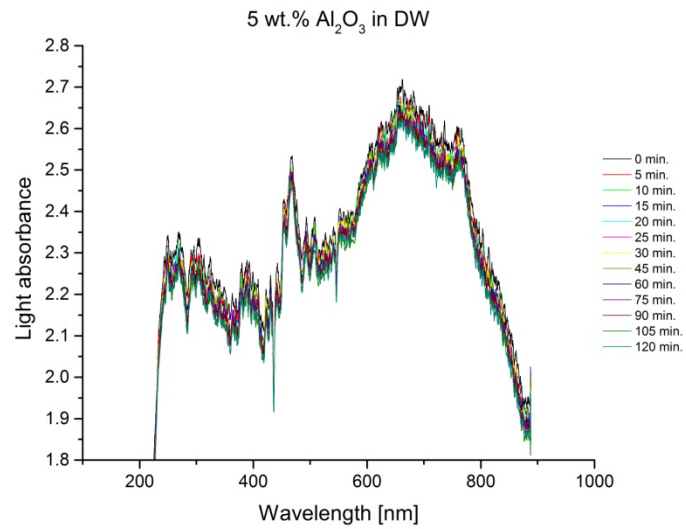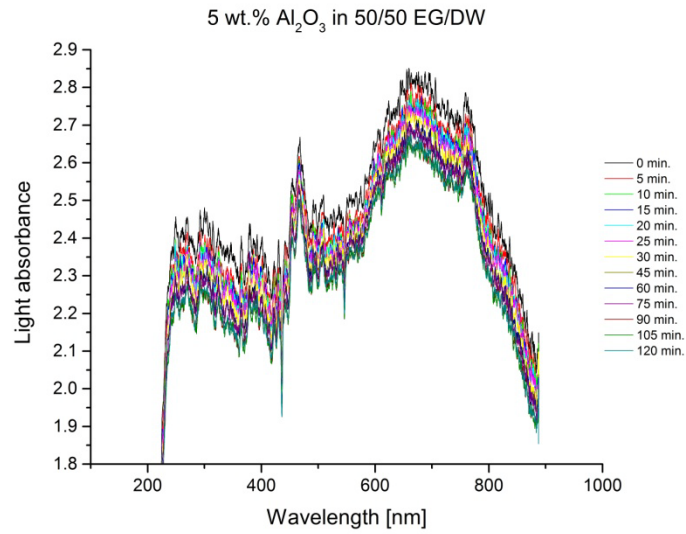
Figure 8. Light absorbance spectrum variation with particle sedimentation time

2.1.6 pH of Nano-fluid

In order to determine the viability of nano-fluid for the real-world application without causing any corrosion to the systems, the pH level of nano-fluids was examined. The nano-fluid samples pH were measured using a pH meter (Mettler Toledo, Model S220) with a 0.001 pH resolution.

2.2 Nano-fluid Property Measurement and Calculation

2.2.1 Thermal Conductivity

The nano-fluid thermal conductivity was measured using a thermal property analyzer device (Decagon Devices, Inc., Model KD2 Pro) based on the transient line heat source method. The accuracy of the sensor is ±5% over the thermal conductivity range of 0.2 W/(m·K) to 2 W/(m·K) and the temperature span of 0°C to 60°C. The device can be set up in auto mode to continuously log measurements at 15 minutes increment. The thermal conductivity was measured at 25°C. Before taking the measurement, a minimum 15-minute time was allowed for nano-fluid sample and sensor to equilibrate them with the testing temperature.

For measuring the thermal conductivity, a setup was designed as shown in Figure 9. It consists of a water bath with outside insulation, an aluminum block for holding the fluid sample and a heating element for controlling the temperature. The water and holding block within the bath create a large thermal mass absorbing the vibration from the surrounding (e.g. HVAC system, laboratory equipment, human activity, etc.) and maintaining a relatively constant temperature. The heating element is used to maintain the water temperature at a desired temperature.
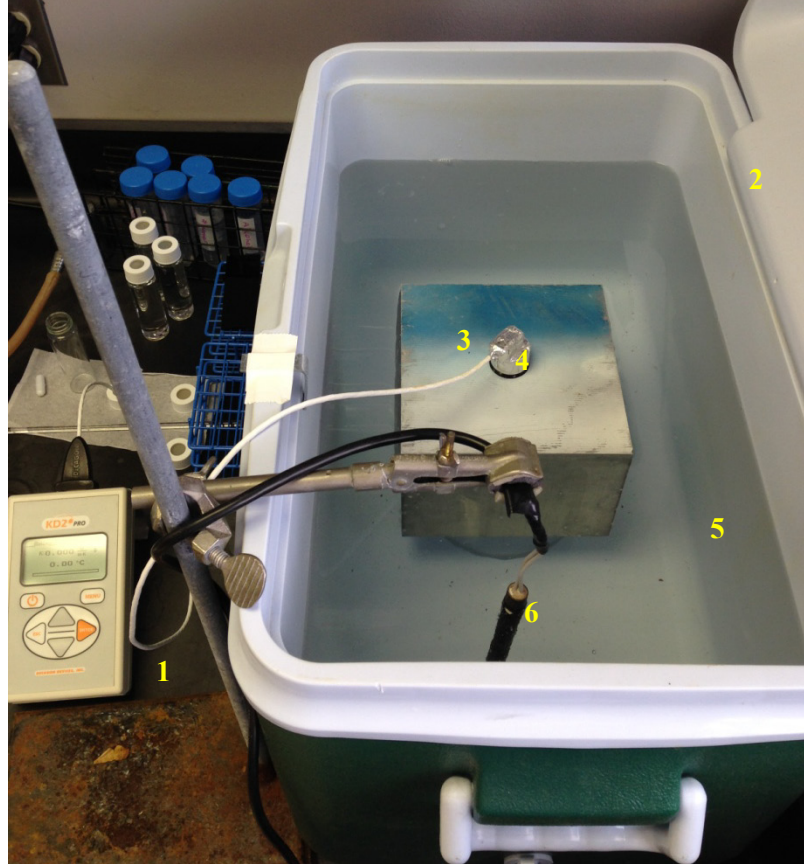
Figure 9. Image of test setup of thermal conductivity test
1. KD2 Pro thermal property analyzer, 2. insulation container, 3. aluminum block, 4. sample vial,
5. water bath, 6. heating element

By using this setup, it was able to measure the thermal conductivity of 50/50 EG/DW up to 60°C. Figure 10 shows the result based on 5 measurements at each temperature. The experimental values fall within ±2% of the theoretical values.
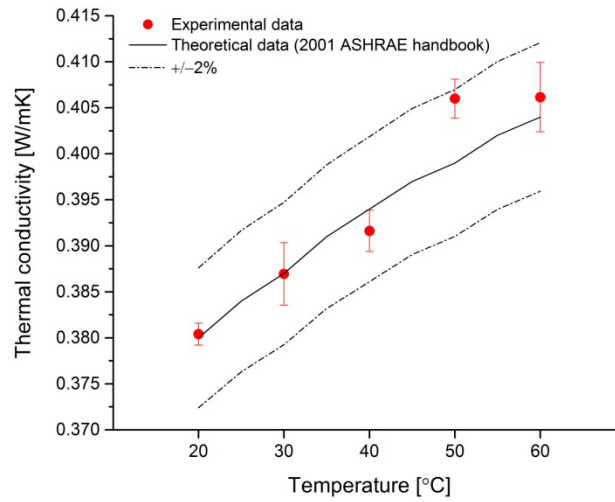
Figure 10. Thermal conductivity measurement of 50/50 EG/DW at various temperatures

2.2.2 Viscosity

The nano-fluid viscosity was measured with the Ubbelohde glass capillary viscometers (PSL Rheotek USA, Inc., Size 0C, 1 and 1B). The viscometer was placed in a temperature controlled water bath in order to measure the viscosity at different temperatures, as shown in Figure 11.
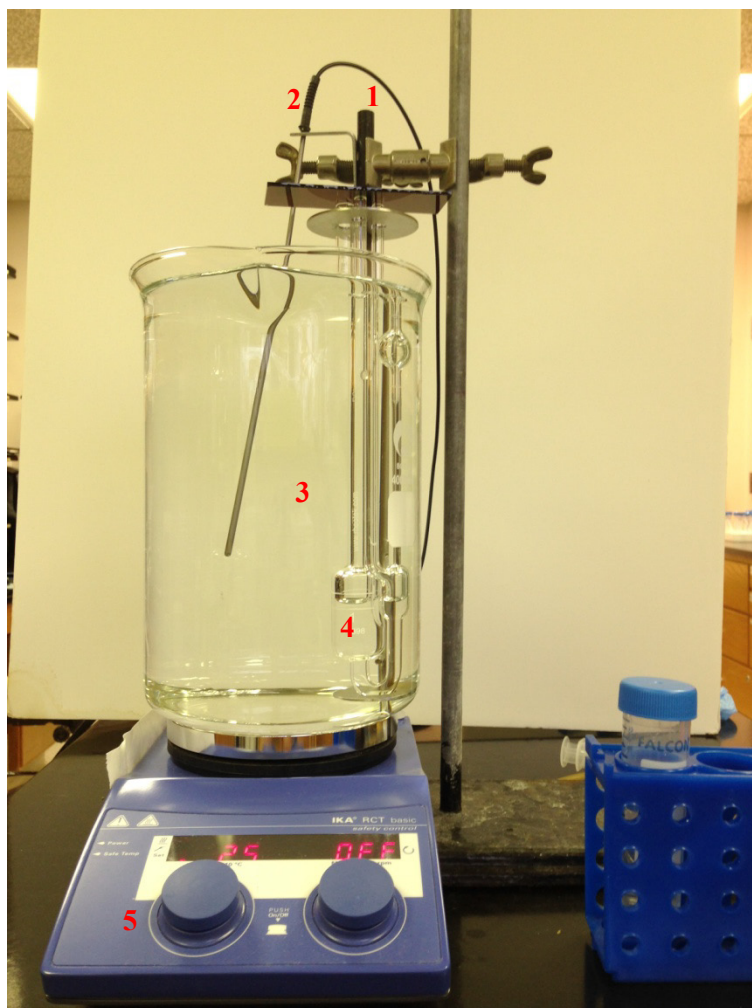
Figure 11. Viscosity measurement setup
1. viscometer stand, 2. hot plate temperature sensor, 3. water bath, 4. viscometer, 5. hot plate with temperature setting display

Figure 12 shows the viscosity measurements of 50/50 EG/DW over the temperature range of 25°C to 65°C. Each data point represents the average value of 5 measurements. As can be seen in Figure 12, the experimental viscosity values fall within ±3% of the theoretical values.
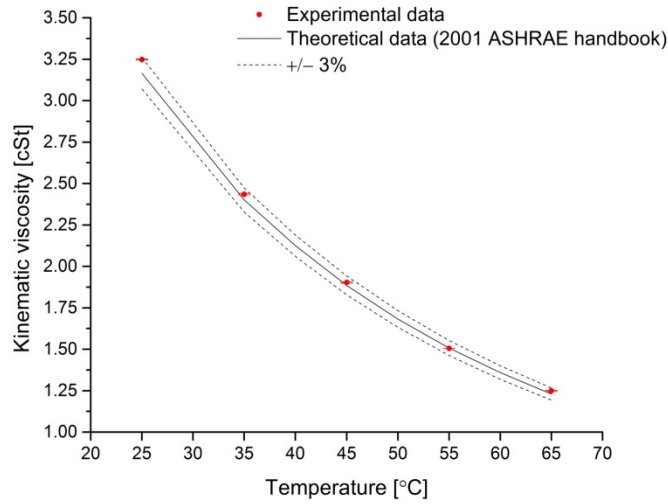
Figure 12. Viscosity measurement of 50/50 EG/DW at various temperatures

2.2.3 Convection Heat Transfer Coefficient

The criteria of designing the nano-fluid convection heat transfer test apparatus is to create the flow condition as the vehicle coolant flows through the radiator. Therefore, the parameters of a vehicle radiator, as shown in Table 1, are used to design the test apparatus.

Table 1. Vehicle radiator parameter

Parameter	Value
Number of heat core tubes	63
Heat core tube width	2 mm
Heat core tube length	18.5 mm
Coolant volumetric flow rate	100 LPM (26.4 GPM)
Coolant temperature at radiator inlet	190˚F (87.8˚C) [32]
Typical coolant temperature difference	10˚C [33]

The Reynolds number of the coolant in the radiator heat core is calculated as [34]

$$Re = \frac{\rho V D_h}{\mu} \qquad (2.1)$$

The Reynolds number is yielded to be 4440. The heat transfer rate for the entire radiator is 70 kW, of which one heat core tube has a 1111.1 W heat transfer rate. The test section of the test apparatus is designed based on a parallel flow double-pipe heat exchanger, in which the tap water in the lab is used as the cooling fluid. The inner tube of the heat exchanger carries the hot nano-fluid, and the annular space of the heat exchanger carries the cooling water. Based on the Dittus-Boelter correlation of the fluid in annuli as [34]

$$Nu = 0.023 Re^{4/5} Pr^n \qquad (2.2)$$

where $n = 0.4$ for heating and $n = 0.3$ for cooling the fluid. The length of the heat exchanging section is determined as 0.8 m. Based on the estimation of the total test apparatus pressure loss with employing a 0.5 inch inner diameter tubing, the requirement of the pump is determined with a capacity to produce up to 2 GPM fluid circulation flow rate.

The schematic of the convection heat transfer test apparatus is shown in Figure 13. It mainly consists of a double-pipe heat exchanger in which the nano-fluid convection heat transfer is tested. The test section is made of a copper tube with a 0.5 inch inner diameter and a 0.625 inch outer diameter. The hydrodynamic entry section is long enough (40 times of the tube inner diameter) to accomplish a fully developed flow at the entrance of the test section. The outer pipe of the double-pipe heat exchanger is made of PVC with a 1.61 inch inner diameter and a 1.9 inch outer diameter. Two T-type thermocouples are placed at the inlet and outlet of the heating and cooling fluids. The testing fluid is heated when it flows through a bended tubing. The tubing is submerged in

a water bath, where the water is heated by a circulation heater. The testing fluid flow rate

is regulated by a needle valve, which is installed at the downstream of the test section,

and a by-pass value, which is installed across the pump. A draining valve is installed at

the inlet of the circulation pump in order to drain the testing fluid. All the temperature

and flow rate sensors are connected to the data acquisition system. It requires 2200 mL of

fluid sample to fill the entire test apparatus in order to run the heat transfer test.
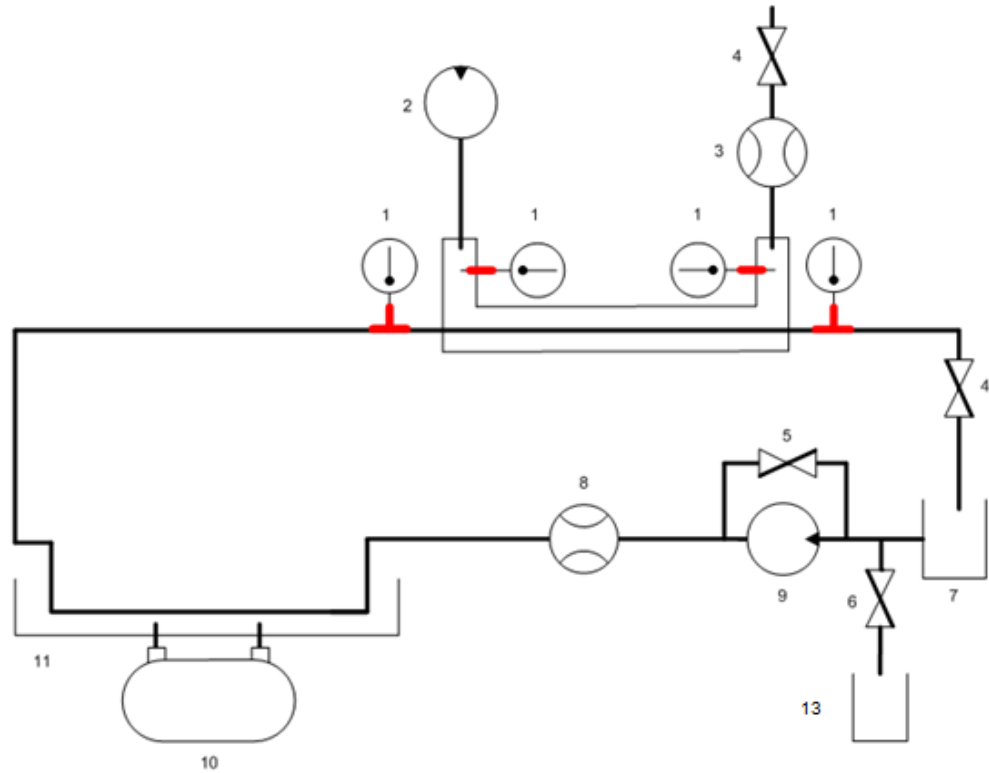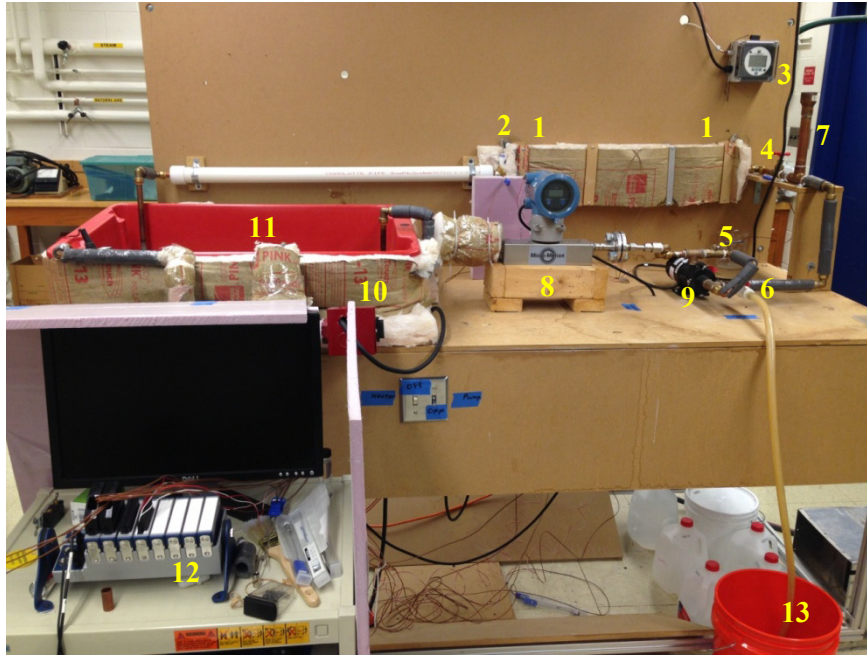
Figure 13. Sketch and photo image of nano-fluid heat transfer test apparatus
1. thermocouple, 2. cooling water inlet, 3. turbine flow meter, 4. flow control valve, 5. flow bypass valve, 6. test apparatus draining valve, 7. test fluid reservoir, 8. Coriolis flow meter, 9. electric pump, 10. heater, 11. water bath, 12. data acquisition system, 13. test fluid collection tank

A Coriolis type flow meter (Micro Motion, Model R025S) is used for measuring the testing fluid flow rate as shown in Figure 14. The flow rate range is from 0.063 GPM to 4.5 GPM. The flow meter accuracy is within ±0.5% of the reading except for when the flow rate is below 0.2405 GPM, where the accuracy decreases to within ±1.9%. The transmitter indicator is configured to have a 4 mA to 20 mA analog signal output. The pressure drop curve of the flow meter is shown in Figure 15.

Figure 14. Coriolis type flow meter (Micro Motion, Model R025S) and transmitter
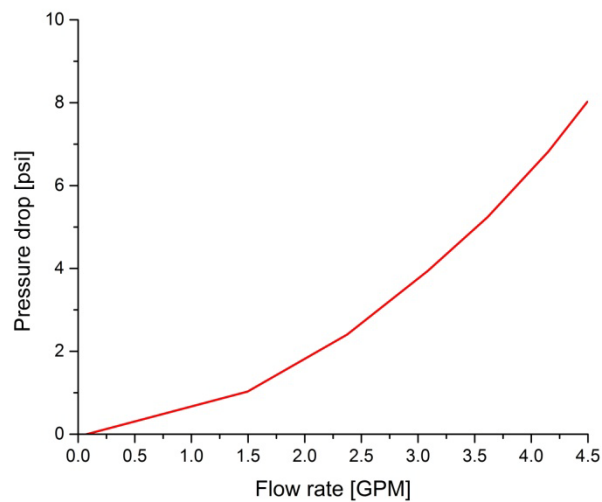
Figure 15. Pressure drop of Coriolis type flow meter (Micro Motion, Model R025S)

A turbine flow meter (Hoffer flow controls, Inc., Model HO 1/2X1/4A) is used for measuring the cooling water flow rate as shown in Figure 16. The flow rate range is from 0.0625 GPM to 4.5 GPM with a ±0.47% accuracy. The flow rate indicator is configured to have a 4 mA to 20 mA analog signal output. The pressure drop curve of the flow meter is shown in Figure 17.

Figure 16. Inline turbine flow meter (Hoffer flow controls, Inc., Model HO 1/2X1/4A) and flow rate indicator
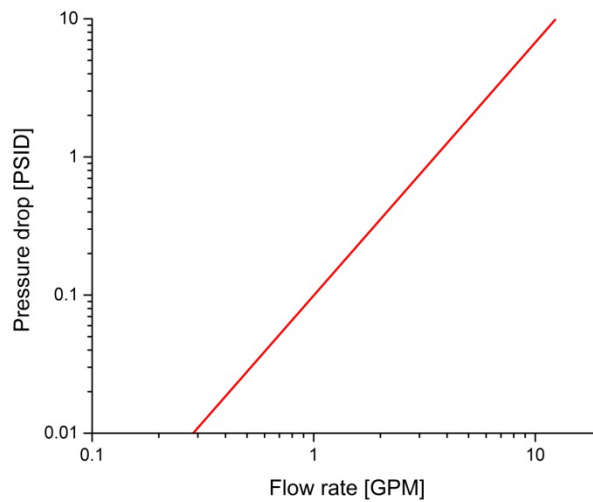
Figure 17. Pressure drop curve of inline turbine flow meter (Hoffer flow controls, Inc., Model HO 1/2X1/4A)

A 105 W magnetic pump (Little giant pump Co., Model 2-MD-HC) is used to circulate the fluid as shown in Figure 18. It can handle fluid temperature up to 90˚C. The pressure rise curve of the pump is shown in Figure 19.

Figure 18. Magnetic pump (Little giant pump Co., Model 2-MD-HC)
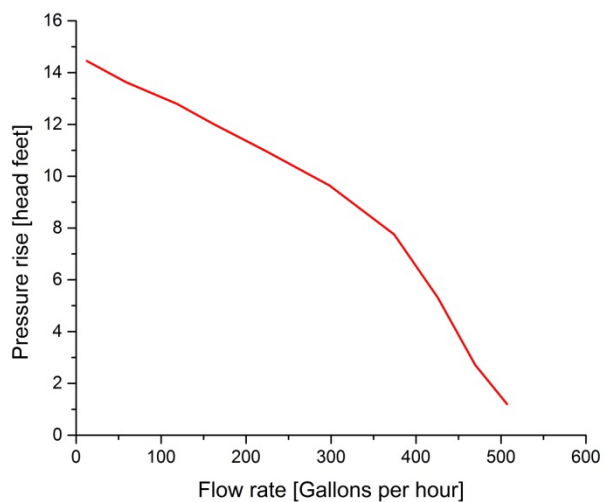
Figure 19. Pressure rise curve of magnetic pump (Little giant pump Co., Model 2-MD-HC)

A 1500 W circulation heater (Hi-Watt Inc., Model PSSB/SCH-15A10), as shown in Figure 20, is used for heating the water bath. The temperature setting of the thermostat is from 16°C to 121°C with a ±4% accuracy.
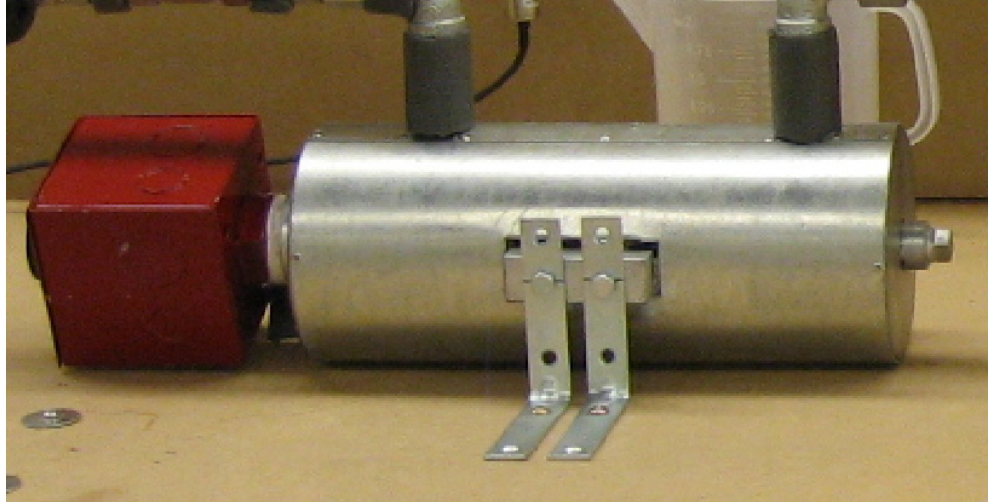
Figure 20. Circulation heater (Hi-Watt Inc., Model PSSB/SCH-15A10)

The T-type thermocouples (Omega, Model TMQSS-062G-6) are used for measuring the fluid temperature as shown in Figure 21. The temperature measurement range is from –270˚C to 400˚C. The output electromotive force (EMF) is from –6.258 mV to 20.872 mV. In the range of 0˚C to 350˚C, the thermocouple accuracy is ±0.75%.

Figure 21. T-type thermocouple (Omega, Model TMQSS-062G-6)

The NI 9213 16-channel thermocouple input module (National Instruments Corporation), as shown in Figure 22, is used to receive the signals from the T-type

thermocouples. It has a ±78.125 mV measurement range, with a 24-bit analog to digital

converter (ADC) resolution for up to 0.02˚C measurement sensitivity.

Figure 22. NI 9213 thermocouple input module (National Instruments Corporation)

The NI 9203 current input module (National Instruments Corporation) is used to

receive the current signal from the flow meters, as shown in Figure 23. It has a 0 mA to

20 mA programmable input range and a 16-bit resolution.

Figure 23. NI 9203 current input module (National Instruments Corporation)

The NI CompactDAQ 9718 USB chassis (National Instruments Corporation) is used to accommodate the NI 9213 and 9203 modules, as shown in Figure 24, which supports LabVIEW (National Instruments Corporation) software for data-logging application.

Figure 24. NI CompactDAQ 9718 USB chassis

A virtual instrument is created in LabVIEW in order to record the thermocouple and flow meter signals as shown in Figure 25. The data is recorded as one sample per second. The output signal of flow meters are scaled to flow rate in LabVIEW, as the 4 mA and 20 mA outputs stand for 0 GPM and 4.5 GPM, respectively.
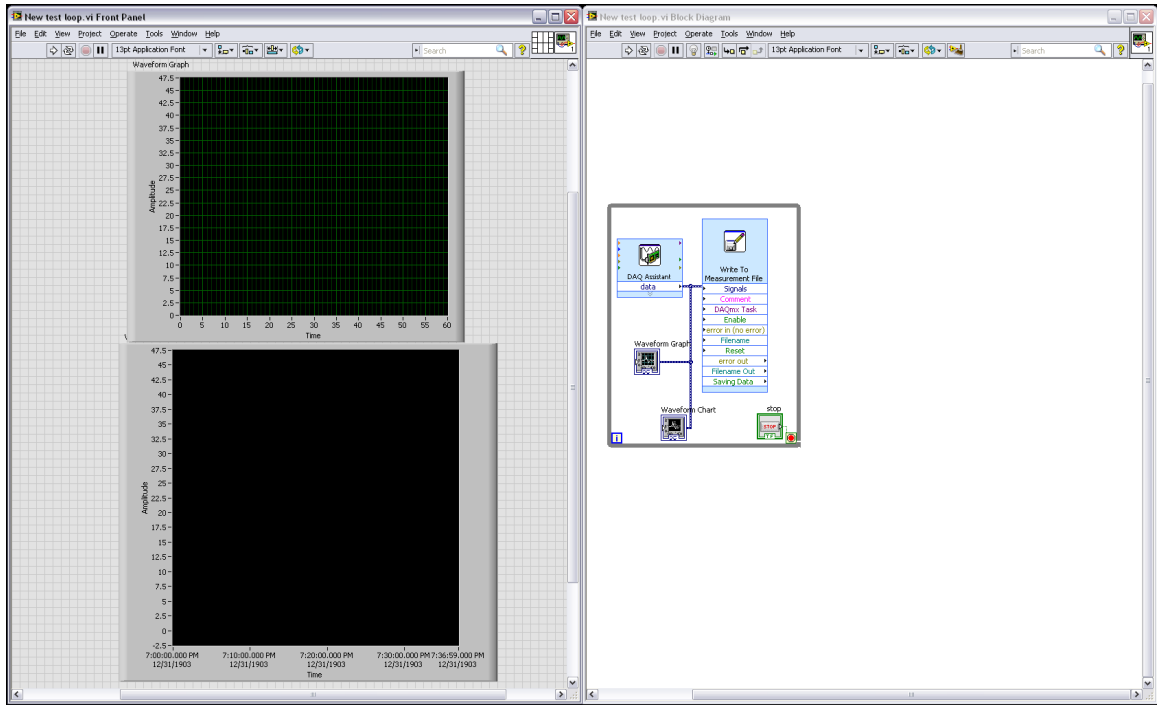
Figure 25. Virtual instrument in LabVIEW

The testing fluid Nusselt number is calculated from the Gnielinski correlation [34],

$$Nu_h = \frac{(f/8)(Re - 1000)Pr}{1 + 12.7(f/8)^{0.5}(Pr^{2/3} - 1)} \qquad \begin{array}{c} 0.5 \leq Pr \leq 2000 \\ 3 \times 10^3 < Re < 5 \times 10^6 \end{array} \qquad (2.3)$$

where the f is determined from the first Petukhov equation [34],

$$f = (0.790 \ln Re - 1.64)^{-2} \qquad (2.4)$$

The theoretical convection coefficient of the testing fluid h_i, as shown in Figure 26, is calculated as [34],

$$h_i = Nu_h \frac{k_h}{D_{i,i}} \qquad (2.5)$$
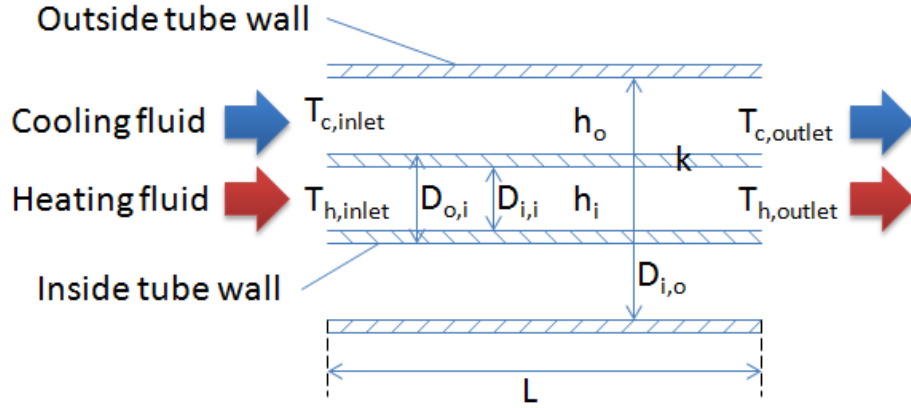
Figure 26. Schematic of the double-pipe heat exchanger

The experimental convection coefficient of the testing fluid $h_{i,exp}$ is calculated based on the thermal resistance analysis of the double-pipe heat exchanger, as shown in Figure 26, as following,

$$\frac{1}{h_{i,exp}} = \frac{1}{U_i} - \frac{D_{i,i} \ln{(D_{o,i}/D_{i,i})}}{2k} - \frac{1}{h_o} \frac{D_{i,i}}{D_{o,i}} \tag{2.6}$$

The overall heat transfer coefficient U_i is determined as [34],

$$U_i = \frac{q}{A_i \Delta T_{lm}} \tag{2.7}$$

The rate of heat transfer from the testing fluid (heating side) is equal to the rate of heat transfer to the cooling water (cooling side), which is,

$$q = \dot{m}_h C_{p,h} \left(T_{h,inlet} - T_{h,outlet} \right) = \dot{m}_c C_{p,c} \left(T_{c,outlet} - T_{c,inlet} \right) \tag{2.8}$$

The inside surface area A_i is calculated as,

$$A_i = \pi D_{i,i} L \tag{2.9}$$

The log mean temperature difference ΔT_{lm} is calculated as,

$$\Delta T_{lm} = \frac{\left(T_{h,inlet} - T_{c,inlet} \right) - \left(T_{h,outlet} - T_{c,outlet} \right)}{\ln{\left[\left(T_{h,inlet} - T_{c,inlet} \right) / \left(T_{h,outlet} - T_{c,outlet} \right) \right]}} \tag{2.10}$$

The cooling fluid convection coefficient h_o is calculated as [34],

$$h_o = Nu_c \frac{k_c}{D_{h,a}} \tag{2.11}$$

The Nusselt number correlations describing the fluid in a smooth concentric annulus during forced convection were proposed by several researchers, as shown in Table 2.

Table 2. Nusselt number correlation of fluid in a smooth concentric annulus in forced convection

Researcher	Equation	Condition
Monrad and Pelton [35]	$Nu_c = 0.02 Re^{0.8} Pr^{0.33} a^{0.53}$ $\quad(2.12)$	$12000 < Re < 22000$ $a = 1.65, 2.45, 17$
Monrad and Pelton [35]	$Nu_c = 0.023 \left[\frac{2\ln a - a^2 + 1}{a - \frac{1}{a} - 2a\ln a}\right] Re^{0.8} Pr^n$ (2.13)	$12000 < Re < 22000$ $a = 1.65, 2.45, 17$ n = 0.4 for heating and n= 0.3 for cooling the fluid
Foust and Christian [36]	$Nu_c = \frac{0.04a}{(a+1)^{0.2}} Re^{0.8} Pr^{0.4}$ $\quad(2.14)$	$3000 < Re < 60000$ $1.2 \leq a \leq 1.84$
Dittus-Boelter [37]	$Nu_c = 0.023 Re^{0.8} Pr^n$ $\quad(2.15)$	n = 0.4 for heating and n= 0.3 for cooling the fluid
Davis [38]	$Nu_c = 0.038 a^{0.15} (a-1)^{0.2} Re^{0.8} Pr^{\frac{1}{3}} \left(\frac{\mu}{\mu_w}\right)^{0.14}$ (2.16)	$1.18 \leq a \leq 6800$
McAdams [39]	$Nu_c = 0.03105 a^{0.15} (a-1)^{0.2} Re^{0.8} Pr^{\frac{1}{3}} \left(\frac{\mu}{\mu_w}\right)^{0.14}$ (2.17)	$1.18 \leq a \leq 6800$
McAdams [39]	$Nu_c = 0.023 Re^{0.8} Pr^{\frac{1}{3}} \left(\frac{\mu}{\mu_w}\right)^{0.14}$ $\quad(2.18)$	
Wiegand [40]	$Nu_c = 0.023 a^{0.45} Re^{0.8} Pr^n \left(\frac{\mu}{\mu_w}\right)^{0.14}$ (2.19)	$1 \leq a \leq 10$ n = 0.4 for heating and n= 0.3 for cooling the fluid

The tube wall surface temperature T_w was calculated as the average of tube inlet and outlet temperatures at the inside surface of inner tube. Figure 27 shows a side view of inlet and outlet of the double pipe exchanger. A steady one-dimensional heat transfer through the inside tube wall of known thickness and thermal conductivity is assumed. The thermal resistance consists of the convection resistance (on the inside tube inner

surface) and the conduction resistance (through the inside tube wall). Based on the inner surface convection resistance analysis, the heat transfer rate q can be calculated as,

$$q = \frac{T_h - T_1}{R_{conv}} = \frac{T_h - T_1}{\dfrac{1}{(2\pi r_{i,i}L)h_i}} \tag{2.20}$$

where the fluid convection heat transfer coefficient h_i is calculated by the Equation (2.5). The heat transfer through the inside tube wall is calculated as,

$$q = \frac{T_1 - T_2}{R_{cyl}} = \frac{T_1 - T_2}{\dfrac{ln\,(r_{o,i}/r_{i,i})}{2\pi L k}} \tag{2.21}$$

Then, the tube wall surface temperature T_w can be calculated as,

$$T_w = \frac{T_{2,inlet} + T_{2,outlet}}{2} \tag{2.22}$$
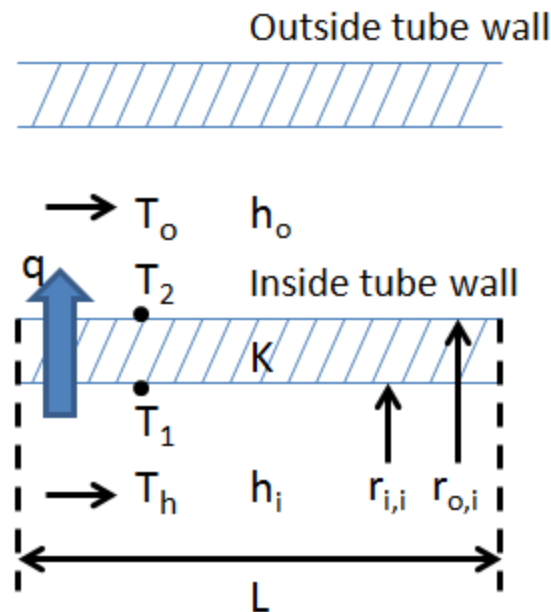
Figure 27. Side view of double-pipe heat exchanger inlet and outlet

Figure 28 shows an example of evaluation of convection heat transfer coefficient of DW. It shows some applications of the Nusselt number correlations in Table 2 well

predict the convection coefficient of DW. The evaluation of the convection coefficient

achieves within ±10% of the theoretical value. Some applications over-estimate or under-

estimate the fluid convection coefficient. It is also found the cooling water condition can

vary the accuracy of Nusselt number correlations in evaluating the testing fluid

convection coefficient. Therefore multiple tests have been conducted to tune the cooling

water condition for the best accuracy.
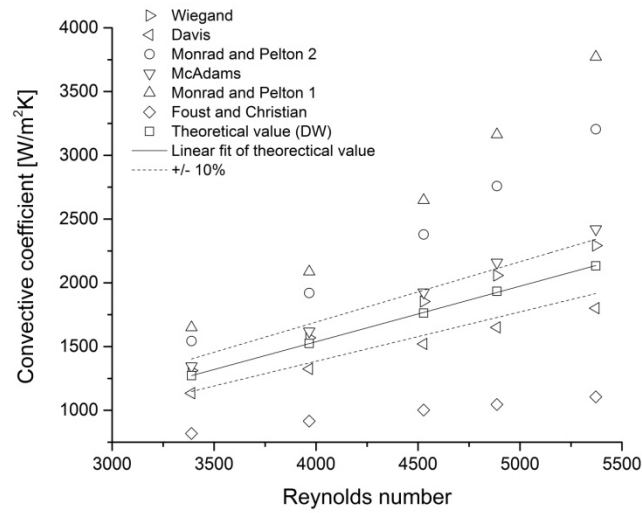
Figure 28. Evaluation of convection heat transfer coefficient of DW

2.2.3 Other Physical Properties

The effective density and specific heat of nano-fluids are estimated as, introduced

by Liu *et al*. [41],

$$\rho_{nf}(T) = \phi\rho_p(T) + (1 - \phi)\rho_{bf}(T) \tag{2.23}$$

$$\left(C_p\right)_{nf}(T) = \phi\left(C_p\right)_p(T) + (1 - \phi)\left(C_p\right)_{bf}(T) \tag{2.24}$$

2.3 Nano-fluid Preparation

Four particle loadings (3, 5, 7 and 9 wt.%) were used when dispersing the nano-particles into different base fluids (DW, EG and 50/50 EG/DW). Base fluid volume was fixed to be 100 mL for each nano-fluid sample. All the particles and base fluids were weighed by an analytical balance (Mettler Toledo, Model AE200) with a 0.0001 g readability.

To prepare the sample, a magnetic stirrer (IKA, Model RCT basic) was used first to stir the sample for about 5 minutes, right after weighed dry nano-powder being poured into the base fluid. Then, a 500 Watts horn-type ultra-sonicator (Qsonica LLC., Model Q500) was used as the main processor to disperse the nano-powder into the base fluid, as shown in Figure 29. The ultra-sonicator was set to operate at 90% amplitude and in a pulse mode (10 seconds on and 10 seconds off). The duration of the ultra-sonication process was set at 60 minutes. Figure 30 shows the variation of particle aggregate size and thermal conductivity enhancement of 5 wt.% Al_2O_3 in 50/50 EG/DW samples processed for different ultra-sonication durations. It indicates that the particle aggregate size reached the minimum level and the thermal conductivity enhancement achieved the maximum level at 60 minutes. However, due to the normal wear of the ultra-sonicator tip, the prolonged ultra-sonication (60+ min.) usually contaminates the sample as a noticeable thin layer of tip debris precipitating at the bottom of the sample after the ultra-sonication process. For ensuring the sample reproducibility, the ultra-sonicator tip condition was examined before the preparation and sample properties were tested at the end of the ultra-sonication process.
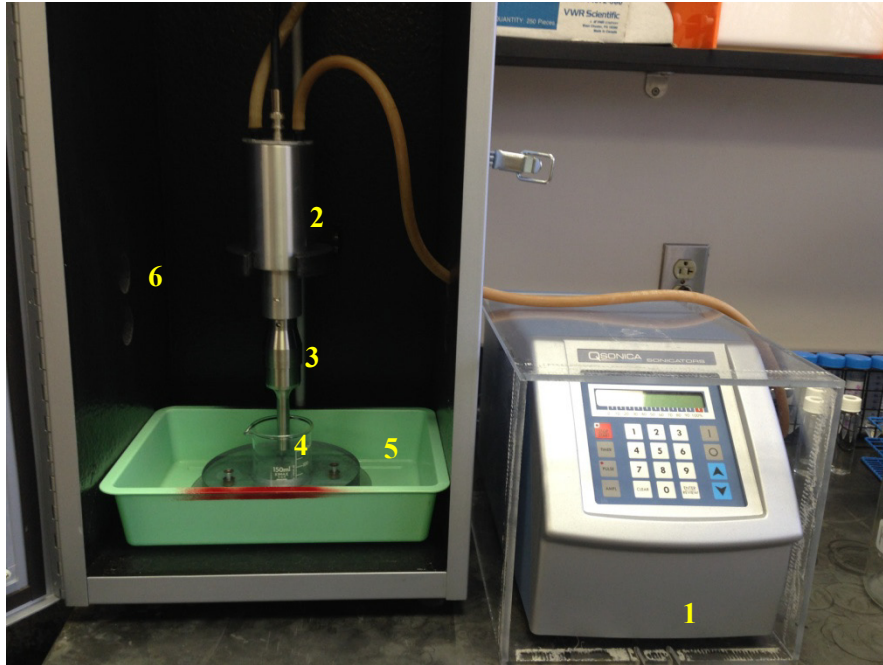
Figure 29. Probe ultra-sonication assembly
1. sonicator generator, 2. sonicator converter, 3. probe, 4. nano-fluid sample, 5. cooling bath, 6. sound enclosure
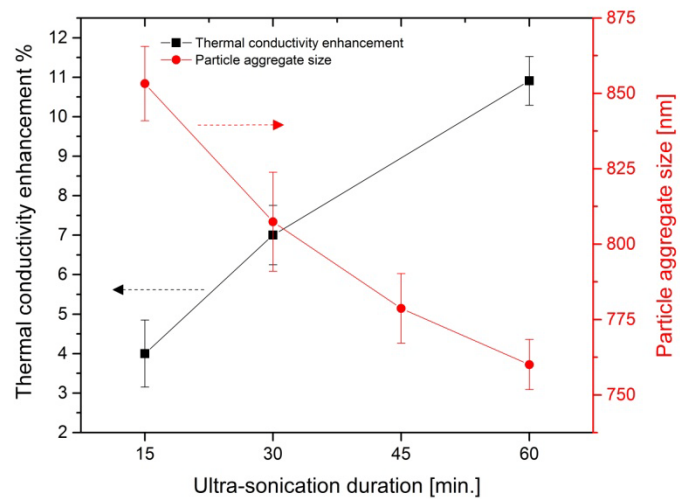
Figure 30. Variation of nano-fluid's particle aggregate size and thermal conductivity enhancement of 5 wt.% Al_2O_3 in 50/50 EG/DW samples processed for different ultra-sonication durations

CHAPTER III

Results and Discussion

3.1 Nano-fluid Property

3.1.1 Effect of Ultra-sonication Duration

The effects of ultra-sonication duration on particle aggregate size variation of 5 wt.% Al_2O_3 dispersed in different base fluids are shown in Figure 31. It indicates that the Al_2O_3 nano-particles are highly aggregated after mixed with the base fluids. The initial particle aggregate size in EG, 50/50 EG/DW and DW were respectively 244,067, 1,512 and 326 nm. The first 15-minute ultra-sonication had the most dramatic aggregate-break-down effect on all the samples, which reduced the particle aggregate size by 50% in EG, by 44% in 50/50 EG/DW and by 54% in DW. The subsequent ultra-sonication broke down the aggregates less efficiently, but it continuously reduced the particle aggregate size to the final minimum level at 60 minute. Figure 31 also shows the difference of overall particle aggregate size between the nano-fluids. In general, the particle aggregates in EG were larger than those in 50/50 EG/DW and DW. The smallest aggregates were found in DW. The aggregates in 50/50 EG/DW were in the middle.
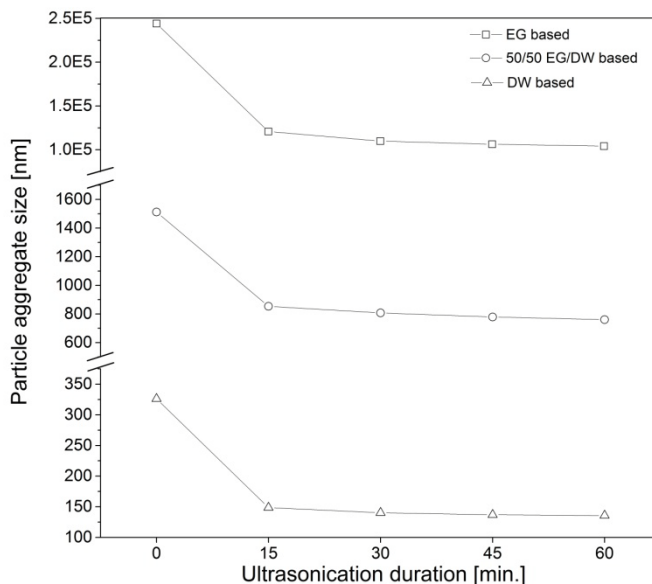
Figure 31. Particle aggregate size variation with ultra-sonication duration of 5 wt.% Al$_2$O$_3$ in different base fluids

3.1.2 Effect of Base fluid

Table 3 shows the correlation between nano-particle aggregation, base fluid viscosity and nano-particle surface charge. It can be seen from the table that the smallest Al$_2$O$_3$ nano-particle aggregate size is achieved with the DW case due to the combined effect of the lowest base fluid viscosity and the highest particle surface charge. The moderate viscosity of 50/50 EG/DW (2.6 times the viscosity of DW) plays a dominant role on the moderate particle aggregation in 50/50 EG/DW. In spite of the fact that the absolute value of particle zeta potential in 50/50 EG/DW is 85% lower than that in DW. The highest aggregation in EG can also be attributed to the combined effect of base fluid viscosity and particle surface charge, in which case EG has the highest viscosity (15.8 times the viscosity of DW) and the absolute value of zeta potential is lowest (94% lower than the value in DW).

Table 3. Correlation between nano-particle aggregation, base fluid viscosity and nano-particle potential

Base fluid	Final particle aggregate size [nm]	Base fluid viscosity [cSt]	Particle zeta potential [mV]
DW	136	0.9	44.75
50/50 EG/DW	760	3.25	6.57
EG	104164	15.17	–2.61

3.1.3 Effect of Nano-particle Aggregation on Nano-fluid Thermal Conductivity Enhancement

Figure 32 shows the thermal conductivity enhancement of 5 wt.% Al_2O_3 nano-particle in the base fluid of EG, DW and 50/50 EG/DW. It indicates that the highest enhancement (10.9%) in thermal conductivity is found in 50/50 EG/DW based nano-fluid, followed by 4.3% enhancement in DW and 4.2% in EG. Figure 32 also shows the final particle aggregate size result from the previous section. It shows that the highest enhancement occurs in 50/50 EG/DW with the moderate particle aggregation. While in the cases of light aggregation in DW and heavy aggregation in EG, the thermal conductivity enhancements are both low. This aggregation-enhancement relation matches with the results of other studies [14, 42] of the particle aggregation effect on the thermal conductivity enhancement, which showed an optimized level of particle aggregation could lead maximum enhancement in thermal conductivity. Being away from the optimized level, either increased or decreased aggregation level would decrease the enhancement.
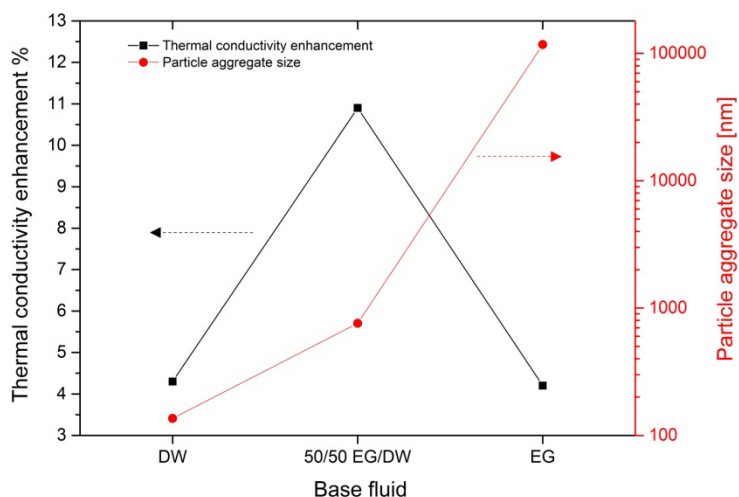
Figure 32. Effect of base fluid on nano-fluid thermal conductivity enhancement

3.1.4 Effect of Nano-particle Concentration

Figure 33 shows the result of thermal conductivity enhancement in different base fluids as a function of Al_2O_3 nano-particle loading, along with the experimental results from other investigators [43-45]. It shows that thermal conductivity enhancement increases as the particle loading increases regardless of the base fluid type. The base fluid effect is also shown in Figure 33, which indicates the enhancements in 50/50 EG/DW based samples are overall higher than those in water and EG based samples in all nano-particle concentrations.

In EG based nano-fluid case, the result from this study shows slightly lower enhancement than that reported by Lee *et al*. [43]. In the water as the base fluid case, the present result of the enhancement in water is among the results claimed by Lee *et al*. [43], Das *et al*. [44] and Eastman *et al*. [45]. Since none of those investigators clearly provided the particle aggregate size at a specific particle loading in their studies, the discrepancy in the thermal conductivity enhancement, as shown in Figure 33, can be explained by the

uncertainty of the different sample preparation methods and thermal conductivity

measuring techniques.
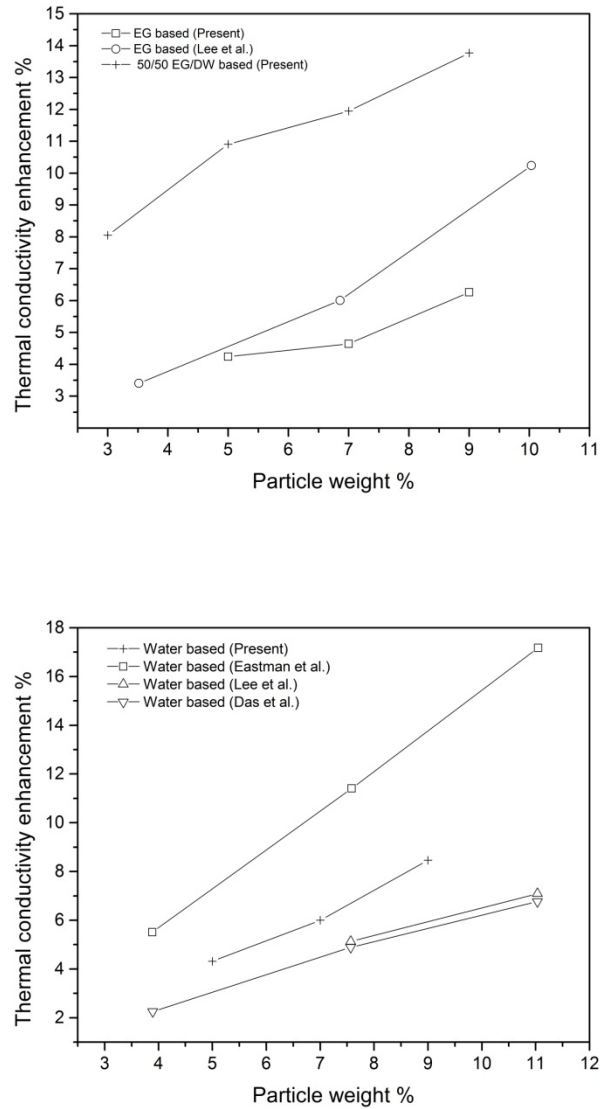
Figure 33. Thermal conductivity enhancement in different base fluids as a function of Al_2O_3 nano-particle loading

3.1.5 Effect of Nano-particle Sedimentation

The particle sedimentation was investigated by measuring the light absorbance of nano-fluid supernatant portion at every 5 minutes for the first 30 minutes and at every 15 minutes for another 90 minutes. This supernatant portion is also the location where the KD2 Pro sensor contacts with the nano-fluid sample for measuring thermal conductivity. Through the investigation, the light absorbance spectra consisting of the single spectrum measured at each specific time were obtained as a function of wavelength. For example, Figure 34 shows the light absorbance spectrum of 5 wt.% Al_2O_3 in 50/50 EG/DW obtained at 0, 30 and 120 minutes. It shows that light absorbance of the supernatant portion decreases with time. By plotting the average light absorbance within a particular wavelength range (i.e. 600 nm to 800 nm) with time, a light absorbance versus time curve was obtained as shown in Figure 35. It offers a more clear view on the sample light absorbance variation over time.

The light absorbance variation curve was further converted to the supernatant particle concentration variation curve, using a linear relationship [46-48] between the light absorbance and the particle concentration as shown in Figure 36. The linear correlation was obtained by calibrating the light absorbance of unsettled samples with different particle concentrations. The pre-determined concentration samples were prepared by diluting 5 wt.% Al_2O_3 in 50/50 EG/DW with specific amounts of base fluid. The above procedure was repeated for the EG and DW based nano-fluids with 5 wt.% Al_2O_3 nano-particle loading, in order to investigate the particle sedimentation effect in those two base fluid cases.

Figure 37 shows the variation of supernatant particle concentration of 5 wt.% Al_2O_3 in different base fluids against the particle sedimentation time. In each case, the

thermal conductivity enhancements at 15 minute intervals for 2 hours were also plotted.

Due to the operational limitation of the KD2 Pro device, the earliest thermal conductivity

enhancement reading can be obtained at 15 minutes. As shown in the Figure 37, after 30

minutes the supernatant particle concentration in DW and 50/50 EG/DW based nano-

fluids both decreased 27.9%, in EG based nano-fluid the decrease was 30.1%. After

another 90 minutes, the supernatant particle concentration decrease in 50/50 EG/DW

based nano-fluid was 22.1% and in DW was 22.2%, while there was little variation in the

supernatant particle concentration in EG based nano-fluid. This would be because of the

higher viscosity of EG which compromised the effect of gravitational force on the rest of

the particles. After 30 minutes, the thermal conductivity enhancement declines in 50/50

EG/DW and DW by 7.5% and 5.5%, respectively. After another 90 minutes the declines

were 4.3% and 4.0%. In these two cases, the percentages of thermal conductivity

enhancement decline were proportional to the percentages of the supernatant particle

concentration loss in the corresponding particle sedimentation period. It indicates that the

particle sedimentation causes the thermal conductivity decline over time. It was also

noticed that the thermal conductivity enhancements of 50/50 EG/DW and DW based

nano-fluids became negative after a certain period time. In the case of EG based sample,

the thermal conductivity enhancement decline was less influenced by the particle

concentration loss in the first 30 minutes. The enhancement decline was 0.8% with the

30.1% loss in particle concentration. The large particle aggregation in EG based sample

may be the reason for this phenomenon. Even when the particle concentration was high,

the enhancement in thermal conductivity was neutralized by the effect of particle heavy

aggregation. While in the rest 90 minutes, the thermal conductivity enhancement didn't decline as the particle concentration stayed at a stable level.
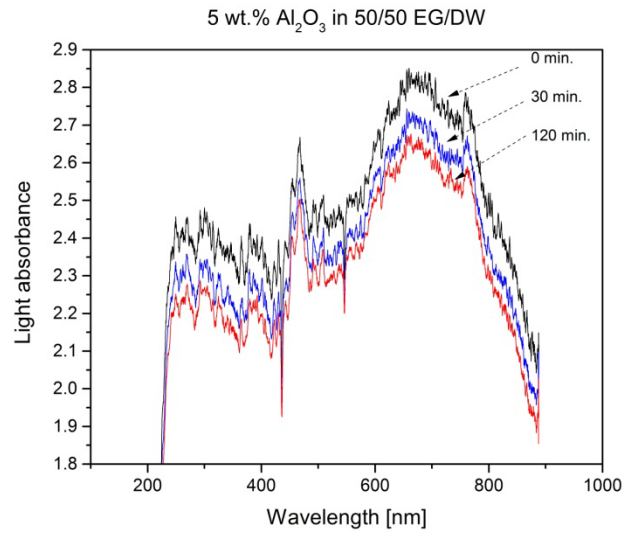
Figure 34. Light absorbance spectrum variation with particle sedimentation time
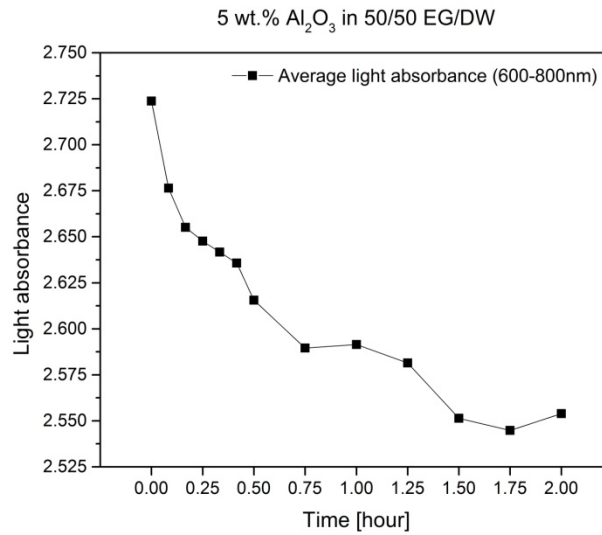
Figure 35. Light absorbance variation with particle sedimentation time
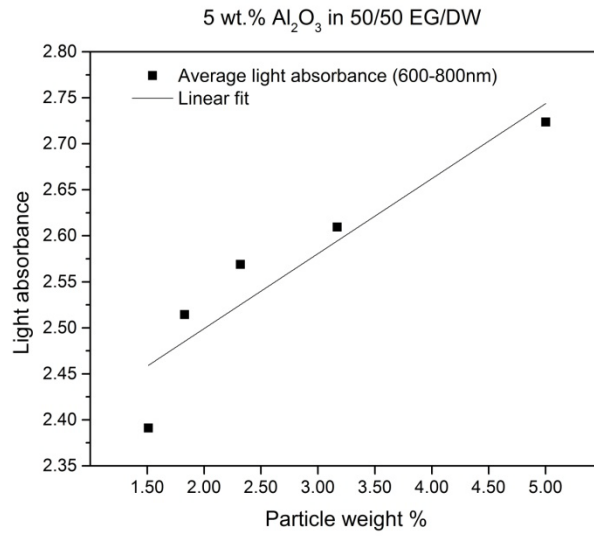
Figure 36. Light absorbance variation as a function of particle loading
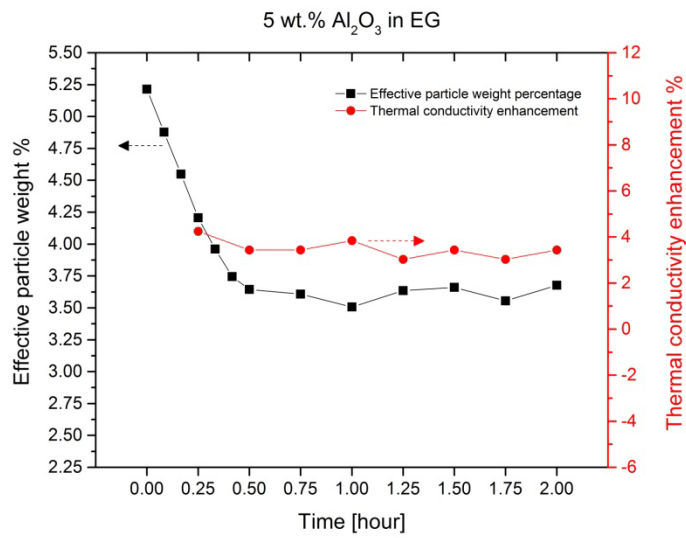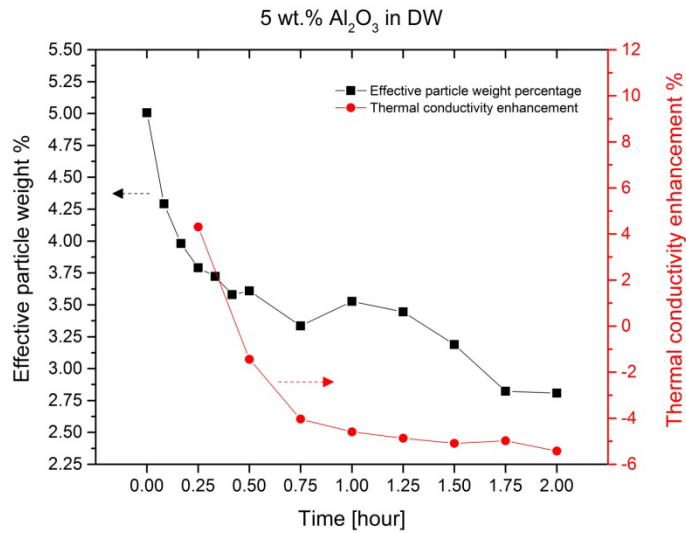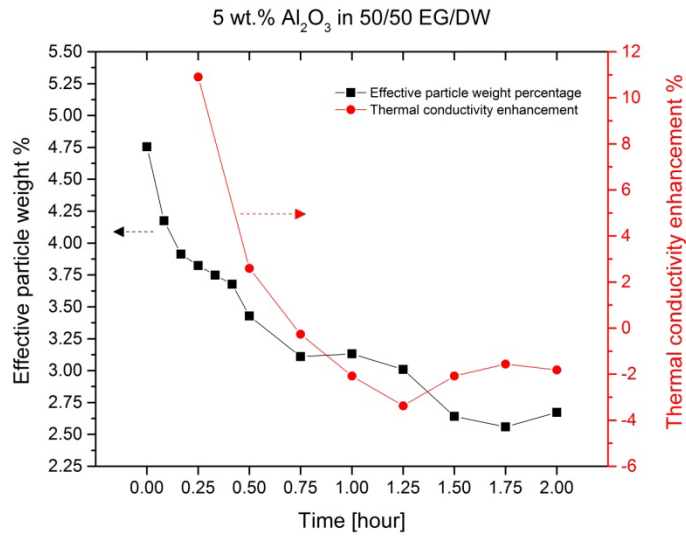
Figure 37. Variation of supernatant particle concentration and thermal conductivity enhancement of 5 wt.% Al$_2$O$_3$ in different base fluids against the particle sedimentation time

3.1.6 Effect of Temperature

The effect of temperature on nano-fluid thermal conductivity was investigated by measuring the nano-fluid thermal conductivity at the temperature range of 25˚C to 35˚C. Figure 38 shows the thermal conductivity of nano-fluid and base fluid versus temperature. Each data point represents the average value of 5 measurements. The base

fluid is 50/50 EG/DW. The nano-fluid is 5 wt.% Al_2O_3 in 50/50 EG/DW. As it can be

seen in Figure 38, the nano-fluid shows thermal conductivity enhancement throughout the

entire testing temperature range. The enhancement ratio shows almost constant over the

temperature range. The KD2 Pro device could not yield reliable readings at higher

temperatures (e.g. 40˚C). The possible reason for the difficulty in getting reliable reading

is that the rapid particle sedimentation in low fluid viscosity environment causes severe

fluid motion, which affects the measurement accuracy. Therefore, the thermal

conductivity of nano-fluid remains uncertain at higher temperature in this study, because

of the measuring limitation of the KD2 Pro device.
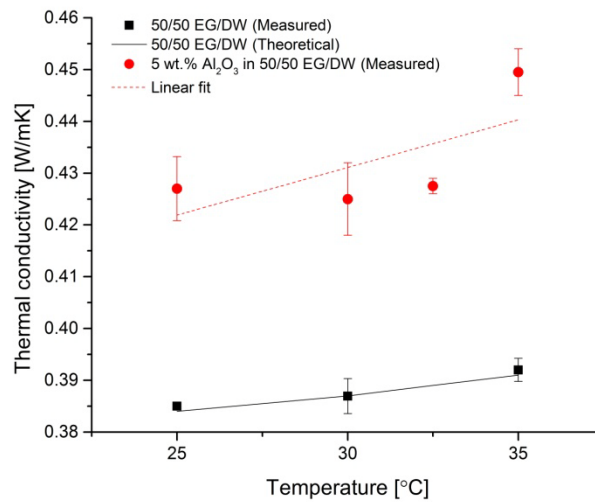
Figure 38. Thermal conductivity of 5 wt.% Al_2O_3 in 50/50 EG/DW versus temperature

Figure 39 shows the viscosity of nano-fluid and base fluid versus temperature.

The viscosity of nano-fluid of 5 wt.% Al_2O_3 in 50/50 EG/DW shows similar behavior as

the viscosity of the base fluid of 50/50 EG/DW, which decreases with the increase in

temperature. The nano-fluid viscosity augmentation percentage over the base fluid

remains at an average value of 6% over the tested temperature range.
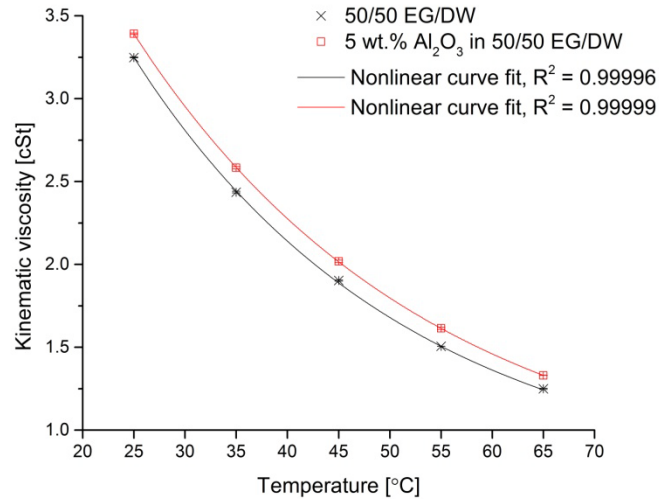
Figure 39. Viscosity of 5 wt.% Al_2O_3 in 50/50 EG/DW versus temperature

3.1.7 Viscosity Augmentation of Nano-fluids

Figure 40 shows the result of nano-fluid viscosity augmentation as a function of

Al_2O_3 nano-particle loading from the three base fluid cases. It shows that EG based nano-

fluid has the highest viscosity augmentation followed by the augmentation in 50/50

EG/DW and DW at the same particle loading. According to the particle aggregate size of

5 wt.% Al_2O_3 based nano-fluids in Table 3, the aggregate sizes in 50/50 EG/DW and EG

were respectively 5.6 and 766 times larger than that in DW, while the percentages of

viscosity augmentation in 50/50 EG/DW and EG were respectively 1.1 and 2.4 times

greater. It can be seen that the viscosity augmentation is related to the particle

aggregation, but the extent of nano-fluid viscosity augmentation over the base fluid is not

proportional to the extent of particle aggregation.
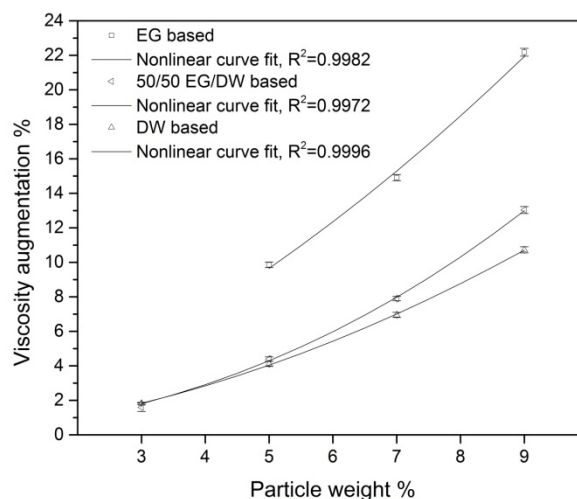
Figure 40. Viscosity augmentation of Al_2O_3 nano-fluids prepared with different base fluids as a function of particle loading

3.1.8 pH of Base fluids and Nano-fluids

The pH of base fluids and nano-fluids are shown in Table 4. The result shows that all the base fluid pH has been changed after the nano-particle dispersion. The largest pH change occurred in the base fluid of EG (from 8.6 to average 4.1) followed by the pH change in base fluid of 50/50 EG/DW (from 7.5 to average 4.4). The least pH change of base fluid was in DW (from 6.6 to average 4.6). However, there is no clear trend showing pH variation with increased particle loading. These pH changes to the base fluid may be caused by the chemical ingredient coming with the Al_2O_3 nano-particle that is acidic. These impurities might also remain suspended after the majority of the nano-particles fell out deteriorating the thermal conductivity enhancement in different base fluids. However, there was no sign of sample color change or particle-base fluid reaction during the period of sample preparation and testing. Therefore, the nano-fluid samples in this study were considered chemically stable.

Table 4. pH value of base fluids and nano-fluids with different Al_2O_3 nano-particle loading

Base fluid	0 wt.%	5 wt.%	7 wt.%	9 wt.%
DW	pH = 6.6	pH = 4.5	pH = 4.6	pH = 4.7
50/50 EG/DW	pH = 7.5	pH = 4.3	pH = 4.4	pH = 4.4
EG	pH = 8.6	pH = 4.1	pH = 4.1	pH = 4.2

3.1.9 Effect of Aging

A test procedure was developed to study the aging effect on nano-fluid characteristics and thermal properties variation, as shown in Figure 41. The particle aggregate size and thermal properties are first measured once the fresh sample is made. The result represents the base line of nano-fluid characteristics and thermal properties. Then, the sample is left stationary at room temperature for 24 hours. The sample is stirred by an overhead stirrer (SCILOGEX, Model OS20-S), as shown in Figure 42, at 1000 rpm for an hour, before the measurements are re-conducted. The overhead stirring process is considered to imitate the scenario of vehicle coolant being stirred by the vehicle coolant pump when the vehicle restarts from a stall. The procedure repeats until the measurements of the 3 days aged sample is conducted.
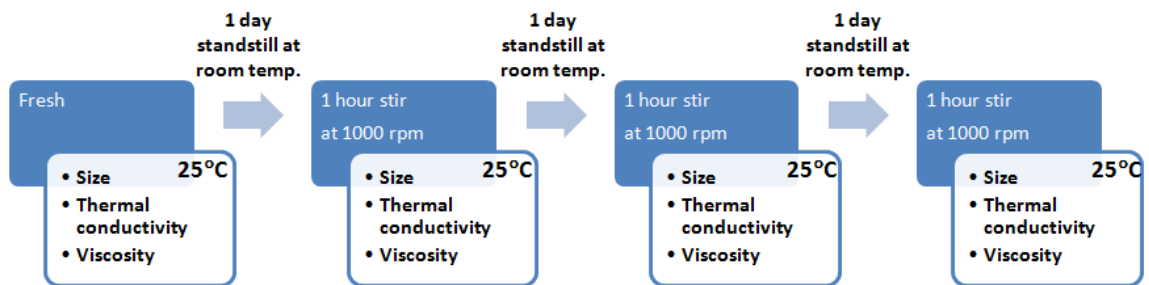
Figure 41. Test procedure of nano-fluid aging effect study
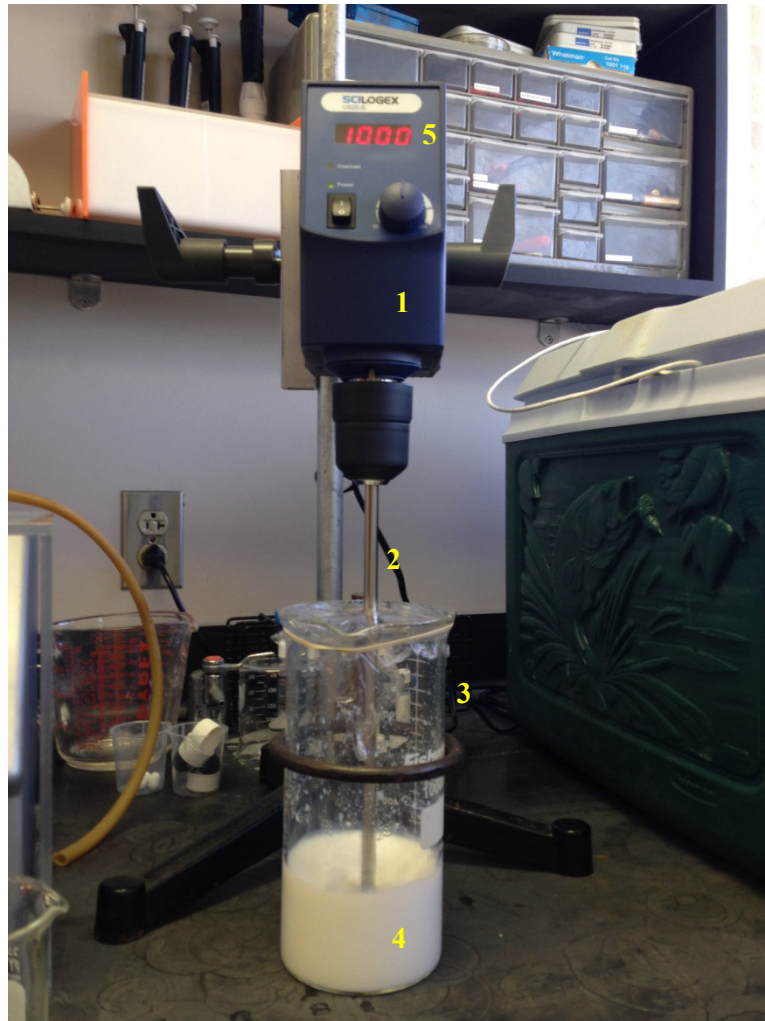
Figure 42. Over-head stirrer assembly
1. stirrer motor, 2. cross stirrer, 3. glass beaker, 4. nano-fluid sample, 5. motor speed display

Figures 43-45 show the aging effect on characteristics and thermal properties variation of a 5 wt.% Al_2O_3 in 50/50 EG/DW nano-fluid. It apparently shows, due to the sample aging, the nano-fluid characteristics and thermal properties are affected. The particle aggregate size increases by 5.8% after 1 day. Also, there is a 1.1% increase in viscosity and 6.1% decrease in thermal conductivity. However, there is no clear trend showing aging effect on further aged samples since there is no dramatic change in characteristics and thermal properties. It indicates the nano-fluid properties can be

maintained at a stable level as long as the stirring is applied. However, the stirring cannot regain the nano-fluid properties at the fresh-sample level.
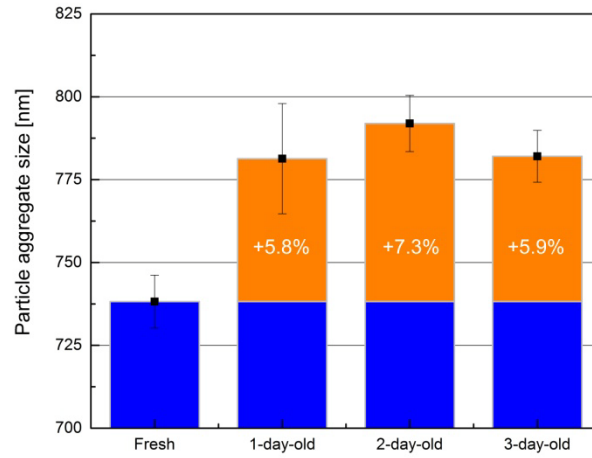
Figure 43. Particle aggregate size variation of 5 wt.% Al_2O_3 in 50/50 EG/DW with sample aging
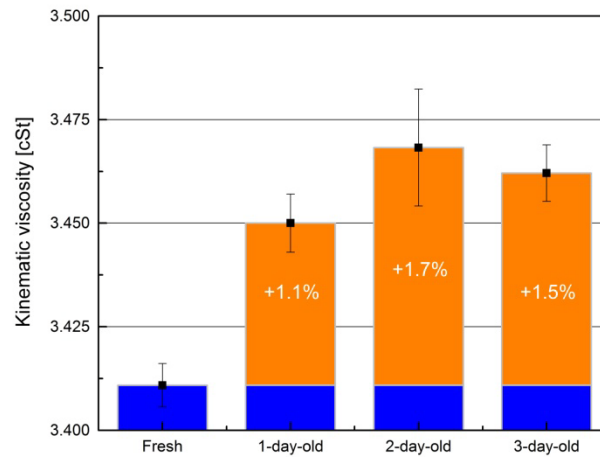
Figure 44. Viscosity variation of 5 wt.% Al_2O_3 in 50/50 EG/DW with sample aging
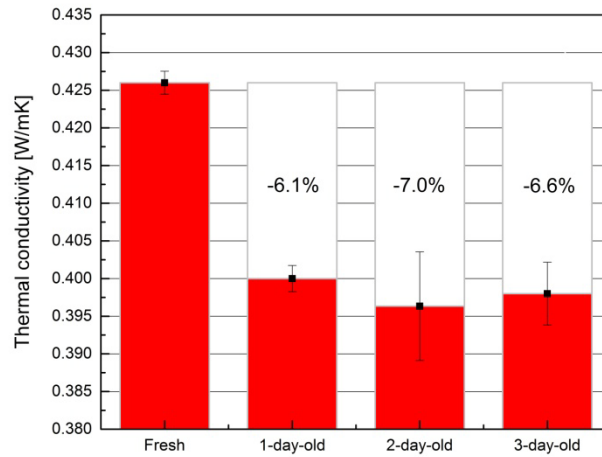
Figure 45. Thermal conductivity variation of 5 wt.% Al_2O_3 in 50/50 EG/DW with sample aging

3.2 Nano-fluid Convection Heat Transfer

3.2.1. Convection Test of Base Fluid

The test procedure of convection heat transfer test is shown in Figure 46.
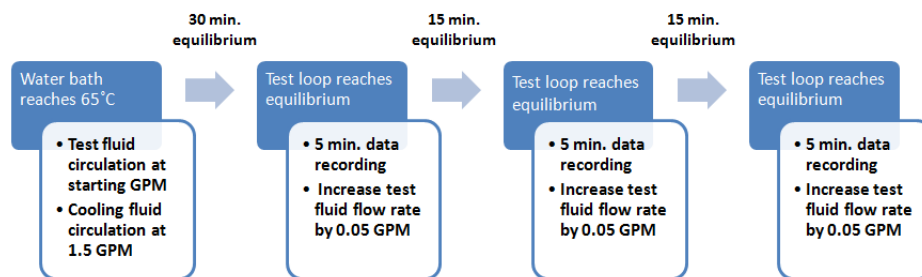
Figure 46. Test procedure of convection heat transfer test

The water bath of the test apparatus, as shown in Figure 13, is first heated to 65°C. Then, the testing fluid is circulated at a relatively low flow rate with the cooling

fluid being delivered to the heat exchanger. When the temperatures and flow rates of the

test apparatus reach the equilibrium state, which usually takes 30 minutes, the data are

recorded for 5 minutes. Then, the testing fluid flow rate is increased by 0.05 GPM, and

data is recorded after the test apparatus reaches the new equilibrium state. The procedure

is repeated increasing the flow rate by 0.05 GPM, until at least 5 data recording cycles are

completed. At each flow rate, the temperature and flow rate represent the average values

of the readings (300 readings) recorded in the 5-minute period. Due to the difference in

the testing fluids viscosities, a wide range of flow rates are tested for each testing fluid,

which makes it possible to compare the convection heat transfer coefficient results

between the different testing fluids in an similar Reynolds number range.

Figure 47 presents the experimental and theoretical convection heat transfer

coefficient results of DW as functions of Reynolds number. The convection heat transfer

coefficients calculated through the experimental measurements mostly fall within ±5% of

the theoretical value obtained by Equation (2.5), which indicates they are in good

agreement.

The heat transfer experiments are also conducted on the 50/50 EG/DW to evaluate

the reliability of the test result. Figure 48 shows the experimental and theoretical

convection heat transfer coefficient results of 50/50 EG/DW as functions of Reynolds

number. It shows that the majority of the experimental value of convection coefficient

falls within ±5% of the theoretical value.
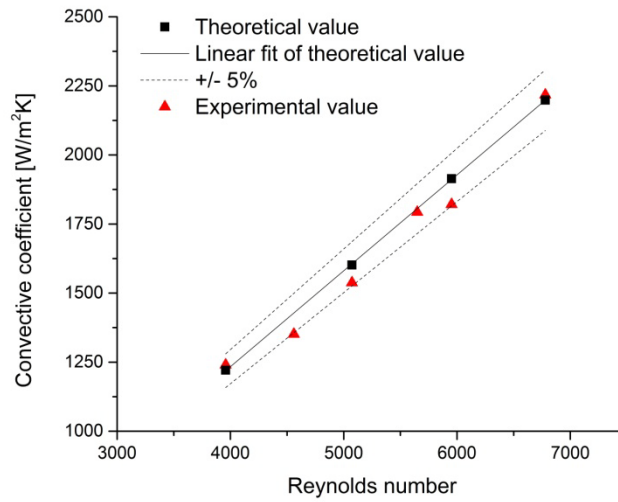
Figure 47. DW convection heat transfer test
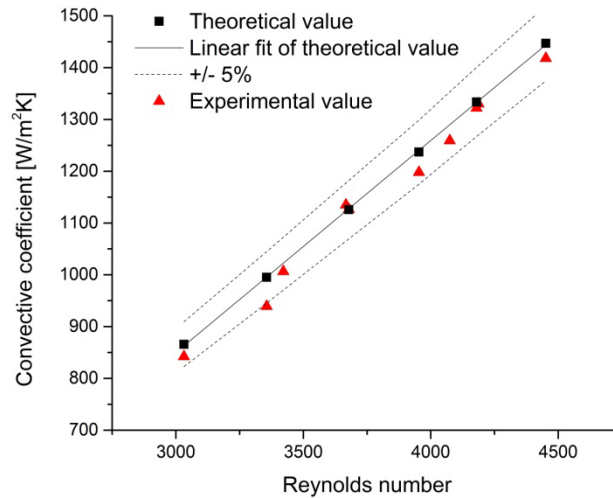
Figure 48. 50/50 EG/DW convection heat transfer test

3.2.2. Convection Test of Nano-fluid

In order to prepare the required amount (2200 mL) of nano-fluid sample for the convection heat transfer test, a standard solid 1" (25 mm) probe (Qsonica LLC., Part No. 4209) with a processing volume range of 100 mL to 1000 mL is employed. A booster (Qsonica LLC., Part No. 4121) is used to double the amplitude of 1" (25 mm) probe,

which has a standard 30 μm amplitude at 100% output. Figure 49 shows the probe ultra-sonication assembly for preparing the heat transfer apparatus test sample. The booster is attached between the sonicator converter and probe. A stir bar running at 500 rpm is applied to assist the sample processing. The ultra-sonicator was set to operate at 100% amplitude and in a pulse mode (10 seconds on and 10 seconds off). The duration of the ultra-sonication process was set at 60 minutes. Two 1100 mL samples are prepared separately before they are mixed together to obtain the 2200 mL sample. Then, the 2200 mL sample is processed under 1-hour ultra-sonication prior to the heat transfer test, which intends to maximize the homogeneous level of the dispersed nano-particles.
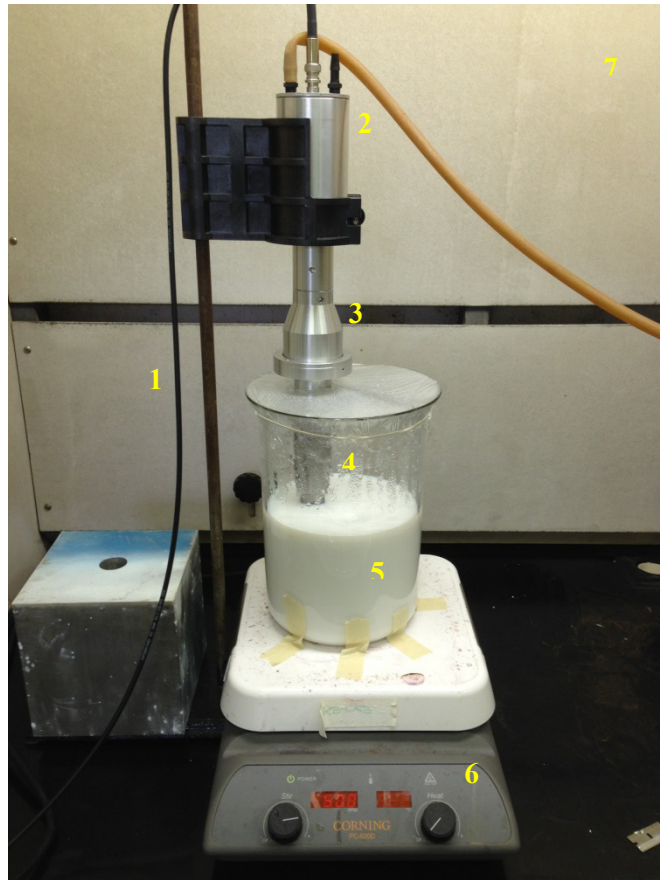
Figure 49. Probe ultra-sonication assembly for preparing the heat transfer apparatus test sample

1. sonicator generator cable, 2. sonicator converter, 3. booster 4. probe, 5. nano-fluid sample, 6. stirrer, 7. fume hood and enclosure

However, the characteristics and thermal properties measurement results of the 2200 mL nano-fluid sample show the sample scale-up production issue. Figure 50 shows the particle aggregate size comparison of fresh 100 mL and 2200 mL samples, which indicates there is a 21% increase in particle aggregate size of the 2200 mL sample. Figure 51 shows the thermal conductivity comparison at 25˚C, which indicates there is a 7.7% decrease in thermal conductivity of the 2200 mL sample. Figure 52 shows the kinematic viscosity comparison at 25˚C, which indicates there is a 5.4% increase in kinematic viscosity of the 2200 mL sample. It is apparent that the scale-up production of nano-fluid in the present study cannot reproduce the thermal properties of small-scale sample (100 mL sample). Once the nano-particle dispersion quality is changed in terms of particle aggregate size, the thermal properties are changed.
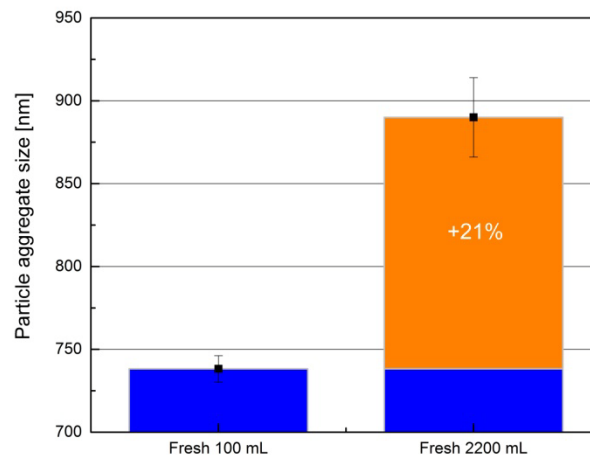
Figure 50. Particle aggregate size comparison of fresh 100 mL and 2200 mL samples
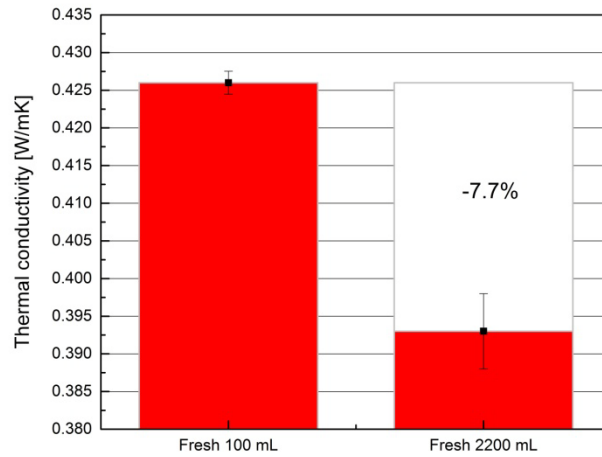
Figure 51. Thermal conductivity comparison of fresh 100 mL and 2200 mL samples at 25˚C
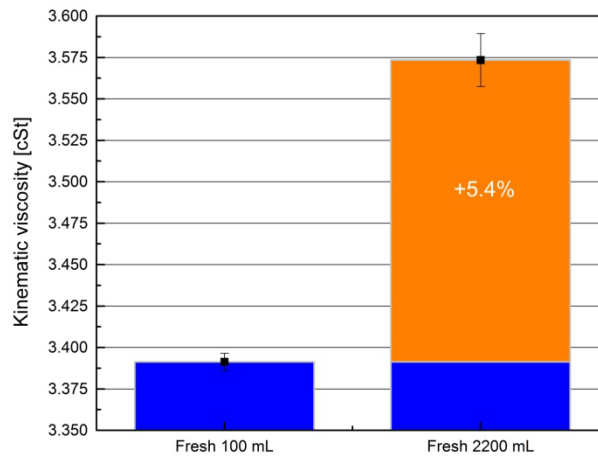
Figure 52. Kinematic viscosity comparison of fresh 100 mL and 2200 mL samples at 25˚C

The convection heat transfer test is conducted to evaluate the 2200 mL sample heat transfer performance. Figure 53 shows the experimental and theoretical convection heat transfer coefficient value of 5 wt.% Al_2O_3 in 50/50 EG/DW versus Reynolds number. The thermal properties value used for calculating the convection heat transfer coefficient is from the sample property measurements at 25˚C. As shown in Figure 53,

the experimental value of nano-fluid convection coefficient falls within ±5% of the theoretical value, which indicates they achieve a good agreement. It also indicates with increase in Reynolds number, the heat transfer coefficient of 5 wt.% Al_2O_3 in 50/50 EG/DW increases.
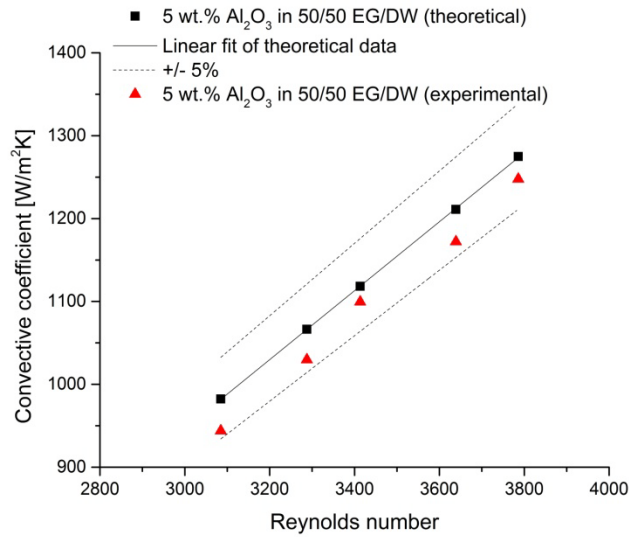
Figure 53. Nano-fluid convection heat transfer test

Figures 54 shows the convection heat transfer coefficients of 5 wt.% Al_2O_3 in 50/50 EG/DW and 50/50 EG/DW versus Reynolds number. As shown in Figure 54, the convection heat transfer coefficient of the nano-fluid increases as much as 10% over the base fluid.
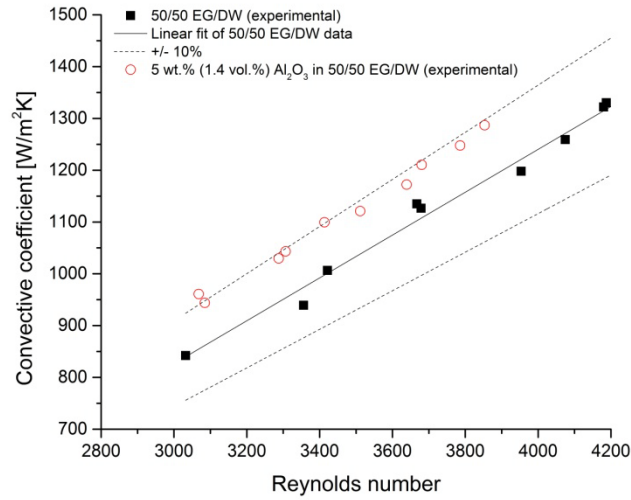
Figure 54. Convection heat transfer coefficients of nano-fluid and base fluid as a function of Reynolds number

Figure 55 shows the average convection heat transfer rates of nano-fluid and base fluid as a function of Reynolds number. The average heat transfer rate is defined as the average value of heating side and cooling side heat transfer rate of the test section. As shown in Figure 55, the average convection heat transfer rates of nano-fluid are higher than the base fluid over the overlapped Reynolds number range.
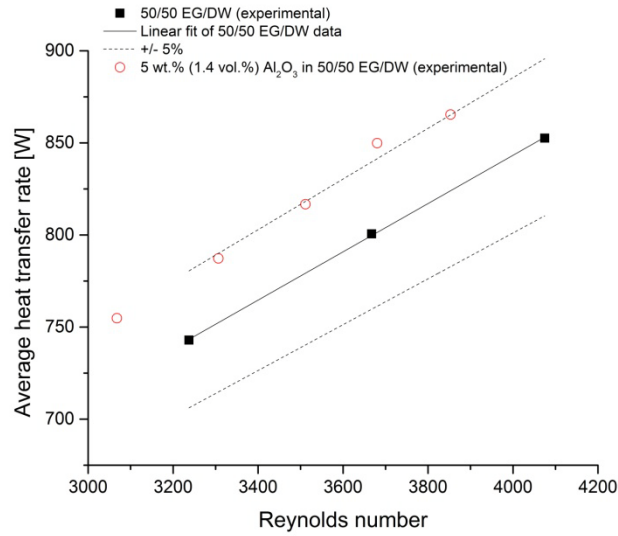
Figure 55. Average convection heat transfer rates of nano-fluid and base fluid as a function of Reynolds number

However, when the average heat transfer rates of the nano-fluid are plotted against flow rate, as shown in Figure 56, it shows a contradicting trend that the nano-fluid average heat transfer rates are close to those of the base fluid.
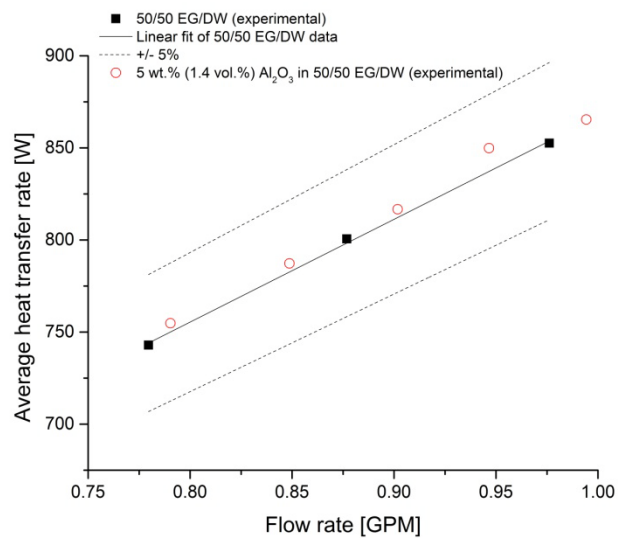
Figure 56. Average convection heat transfer rates of nano-fluid and base fluid as a function of flow rate

An example of recorded convection heat transfer test data is listed in Table 5 in order to compare the heat transfer performance between nano-fluid and base fluid at the same flow condition. The comparison shows nano-fluid has a close performance as the base fluid in terms of convection heat transfer.

Table 5. Example of recorded test data of convection heat transfer test

Test	Fluid	Cooling side		
No.	Name	Flow rate [GPM]	Inlet temperature [˚C]	Outlet temperature [˚C]	Temperature difference [˚C]
1	Nano-fluid	1.47	10.36	12.36	2.00
	Base fluid	1.54	11.87	13.79	1.92
2	Nano-fluid	1.47	9.82	11.96	2.14
	Base fluid	1.52	11.25	13.32	2.07
3	Nano-fluid	1.52	9.75	11.90	2.15
	Base fluid	1.53	10.77	12.94	2.17

Test	Fluid	Heating side		
No.	Name	Flow rate [GPM]	Inlet temperature [˚C]	Outlet temperature [˚C]	Temperature difference [˚C]
1	Nano-fluid	0.78	58.78	54.72	4.06
	Base fluid	0.78	56.53	52.55	3.98
2	Nano-fluid	0.87	58.20	54.23	3.97
	Base fluid	0.88	56.77	52.92	3.85
3	Nano-fluid	0.99	56.82	53.11	3.71
	Base fluid	0.98	56.63	52.90	3.73

The above results show, when the nano-fluid average convection heat transfer rates are plotted against different parameters, there are contradicting trends of heat transfer performance between nano-fluid and base fluid. In convection heat transfer rate versus Reynolds number plot, the fluid pumping power penalty caused by the viscosity argumentation in nano-fluid does not dominate the relationship between its convection

heat transfer rate and Reynolds number, since the Reynolds number is not only a function of fluid viscosity but also a function of fluid density and flow rate. When the nano-fluid Reynolds number reaches the same region of that of the base fluid, which is realized by increasing the fluid pumping power, the nano-fluid has higher heat transfer performance than the base fluid. However, in convection heat transfer rate versus flow rate plot, the pumping power penalty dominates the relationship between nano-fluid convection heat transfer rate and flow rate. At the same flow rate, the nano-fluid has a convection heat transfer performance close to the base fluid.

Additional tests have been conducted at lower temperature by lowering the water bath temperature to 40°C. Table 6 is an example of recorded test data of convection heat transfer test. It shows, at the same fluid condition, there is no difference in heat transfer performance between the nano-fluid and the base fluid.

Table 6. Example of recorded test data of convection heat transfer test

Test	Fluid	Cooling side		
No.	Name	Flow rate [GPM]	Inlet temperature [°C]	Outlet temperature [°C]	Temperature difference [°C]
1	Nano-fluid	1.47	19.34	20.10	0.76
	Base fluid	1.50	18.84	19.60	0.77
2	Nano-fluid	1.57	19.29	20.07	0.78
	Base fluid	1.54	18.60	19.41	0.81
3	Nano-fluid	1.56	19.04	19.85	0.81
	Base fluid	1.51	18.67	19.49	0.82

Test	Fluid	Heating side		
No.	Name	Flow rate [GPM]	Inlet temperature [°C]	Outlet temperature [°C]	Temperature difference [°C]
1	Nano-fluid	1.01	38.49	37.24	1.25
	Base fluid	0.98	38.10	36.86	1.24
2	Nano-fluid	1.11	38.56	37.31	1.24
	Base fluid	1.10	38.17	36.93	1.24

3	Nano-fluid	1.15	38.48	37.24	1.24
	Base fluid	1.14	38.17	36.93	1.24

Further tests have been conducted after the sample is circulated in the test apparatus at maximum flow rate and room temperature for 24 hours. The 24-hour circulation is expected to break down the particle aggregates to improve the nano-fluid sample in terms of regaining the thermal properties of the small-scale sample (100 mL sample). The results do not show any improvement in convection heat transfer performance of nano-fluid. The heat transfer result shows the same performance as the uncirculated sample.

Further measurements are conducted on the convection heat transfer coefficient of Al_2O_3 in 50/50 EG/DW at different weight concentrations (3 and 7 wt.%) of nano-particle. Figure 57 shows the convection heat transfer coefficient of Al_2O_3 in 50/50 EG/DW with varying nano-particle concentration and 50/50 EG/DW versus Reynolds number. As shown in Figure 57, the convection heat transfer coefficients of Al_2O_3 in 50/50 EG/DW with different nano-particle weight concentrations are higher than those of the base fluid. The heat transfer coefficient of Al_2O_3 in 50/50 EG/DW also increases with nano-particle weight concentration.
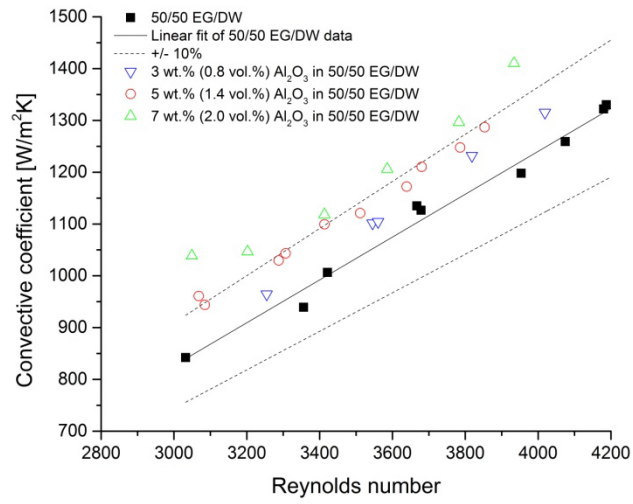
Figure 57. Nano-fluid convection heat transfer coefficient versus Reynolds number

CHAPTER IV

Summary and Conclusion

In this study, Al_2O_3 nano-particle based nano-fluids have been investigated thoroughly through the characterization, thermal property and convection heat transfer performance study. A commercially available Al_2O_3 nano-particle has been dispersed at various concentration in distilled water, ethylene glycol and ethylene glycol/distilled water (50/50 vol.%) mixture. Two-step method was used for the sample preparation in which the magnetic stirrer and horn-type ultra-sonicator were employed.

In the characterization and thermal property study, the nano-fluid samples were characterized by the TEM imaging, particle surface charge (zeta potential), particle aggregate size, light absorbance and pH. The thermal physical properties (thermal conductivity and viscosity) of the nano-fluid samples were measured at various temperatures. The particle sedimentation behavior was observed. The effect of aging on the nano-fluid thermal properties was studied. The following conclusions were made through the study:

1. The duration of ultra-sonication process was optimized to 60 minutes through the study. A prolonged ultra-sonication process may cause sample contamination.

2. The Al_2O_3 nano-particle aggregation in different base fluids was determined by the combined effect of the base fluid viscosity and the particle surface charge (zeta potential).

3. The effect of particle aggregation on the nano-fluid thermal conductivity enhancement was discussed, when three different types of base fluids were investigated with the 5 wt.% Al_2O_3 nano-particle loading. The high thermal conductivity enhancement (10.9%) in 50/50 EG/DW could be attributed to the moderate particle aggregation (final particle aggregate size is 760 nm). Either light or heavy particle aggregation (final particle sizes are respectively 136 nm and 104164 nm in DW and EG) could lower the thermal conductivity enhancement (4.3% enhancement in DW and 4.2% in EG). With nano-particle loading up to 9 wt.%, the ethylene glycol/distilled water (50/50 vol.%) mixture based nano-fluids showed overall higher thermal conductivity enhancement than the distilled water and ethylene glycol based nano-fluids.

4. The nano-fluid thermal conductivity enhancement over the base fluids increased with increase in nano-particle loading.

5. The nano-fluid thermal conductivity enhancement decline was correlated with the gravity-driven particle sedimentation.

6. Nano-fluid viscosity augmentation over the base fluid was related to the particle aggregation which showed nano-fluids containing larger particle aggregates had higher viscosity augmentation over the base fluid. However, the extent of viscosity augmentation was not proportional to the extent of particle aggregation.

7. The impurity of the Al_2O_3 nano-powder was noticed through the nano-fluid pH change against the base fluid measurement. This impurity may cause the nano-fluid thermal conductivity below the base fluid level, after the majority of the nano-particles fell out of the nano-fluid.

8. The thermal conductivity and viscosity of Al_2O_3 nano-particle based nano-fluid showed temperature dependence over the tested temperature range. However the thermal conductivity enhancement ratio (nano-fluid thermal conductivity versus base fluid thermal conductivity) and viscosity augmentation ratio (nano-fluid viscosity versus base fluid viscosity) remained same over the tested temperature range.

9. Nano-fluid sample aging showed an irreversible effect on changing the sample characteristics and thermal properties, when the 5 wt.% Al_2O_3 nano-particle based 50/50 EG/DW nano-fluid was investigated. The one day aged sample showed 5.8% increase in particle aggregate size, 6.1% decline in thermal conductivity and 1.1% augmentation in viscosity. However the changes could be maintained at a stable level as long as the mechanical stirring was applied to the nano-fluid sample.

The forced convection heat transfer performance of nano-fluid in the Reynolds number range of 3000 to 4000 was studied through a specially designed heat transfer apparatus. Nano-fluid sample for the heat transfer test were prepared differently by a scale-up production method. The characteristics and thermal properties of the sample were measured before the sample was loaded into the test apparatus. The following conclusions were made through the study:

1. The scale-up production of the large nano-fluid sample (2200 mL) showed challenge in regaining the thermal properties of the small sample (100 mL). The sample made by the scale-up production has larger nano-particle aggregates, lower thermal conductivity enhancement and greater viscosity augmentation than the sample made by the small scale production.

2. The convection heat transfer performance comparisons between the nano-fluid and the base fluid showed contradicting trends when the comparisons were conducted in different parameter based plots. Nano-fluid showed higher convection heat transfer rates over those of the base fluid in the Reynolds number based plot, while it showed close heat transfer rates to those of the base fluid in the flow rate based plot.

3. Due to the viscosity augmentation of nano-fluid over the base fluid, the pumping power penalty dominated the relationship between nano-fluid convection heat transfer rate and flow rate. It caused the convection heat transfer performance of nano-fluid close to the base fluid performance.

CHAPTER V

Suggested Future Work

Since the scale-up production of the Al_2O_3 nano-particle based nano-fluid in the current study was not successful to reproduce the thermal properties of the small amount (100 mL) sample, it will be valuable to develop an efficient way for the mass production of the nano-fluid. On the other hand, it is still possible to develop the convection heat transfer coefficient correlation of the sample made by the small-scale production, by testing the sample in a test apparatus requiring small amount of sample (<100 mL). One of the viable designs will be a small circulation loop consisting of a micro-channel, which can be potentially used for the electronics cooling applications.

The irresistible aging effect on the Al_2O_3 nano-particle based nano-fluid properties requires stability improvement of the particle-fluid system in order to maintain the nano-fluid functionality.

Since there is only one specific type of nano-particle material (Al_2O_3) is selected for nano-fluid synthesis in this study, it will be viable to change the material-wise parameters for the nano-fluid characterization and behavior investigation. Al_2O_3 nano-particles with a wide range morphology (shape and size) are commercially available. The new testing matrix can be designed by fixing one parameter to study the effect of varying another parameter (e.g. fixing nano-particle shape and varying nano-particle size, or vise versa).

Furthermore, instead of using Al_2O_3 nano-particle, different nano-particle materials can be studied. There is a wide variety of nano-particles available. The surface properties of nano-particles could be quite different, which results in the different nano-particle dispersibility in the base fluids. And, it will eventually exhibit the difference in nano-fluid stability. It is possible to find the most stable nano-fluid with the relatively low-cost nano-particle material through tremendous research efforts.

REFERENCE

[1] J. C. Maxwell, *A Treatise on Electricity and Magnetism*, 2nd ed. Oxford, U.K.: Clarendon Press, 1881.

[2] Y. Xuan, and Q. Li, "Heat transfer enhancement of nanofluids," International Journal of Heat and Fluid Flow, vol. 21, no. 1, pp. 58-64, Feb. 2000.

[3] S. U. S. Choi, Z. G. Zhang, W. Yu, F. E. Lockwood, and E. A. Grulke, "Anomalous thermal conductivity enhancement in nanotube suspensions," Applied Physics Letters, vol. 79, no. 14, pp. 2252-2254, Oct. 2001.

[4] J. A. Eastman, S. U. S. Choi, S. Li, W. Yu, and L. J. Thompson, "Anomalously increased effective thermal conductivities of ethylene glycol-based nanofluids containing copper nanoparticles," Applied Physics Letters, vol. 78, no. 6, pp. 718-720, Feb. 2001.

[5] H. E. Patel, S. K. Das, T. Sundararajan, A. S. Nair, B. George, and T. Pradeep, "Thermal conductivities of naked and monolayer protected metal nanoparticle based nanofluids: manifestation of anomalous enhancement and chemical effects," Applied Physics Letters, vol. 83, no. 14, pp. 2931-2933, Oct. 2003.

[6] D. J. Faulkner, D. R. Rector, J. J. Davidson, and R. Shekarriz, "Enhanced heat transfer through the use of nanofluids in forced convection," in Proceedings of the 2004 ASME International Mechanical Engineering Congress and Exposition, Anaheim, CA, 2004, pp. 219-224.

[7] Y. Ding, H. Alias, D. Wen, and R. A. Williams, "Heat transfer of aqueous suspensions of carbon nanotubes (CNT nanofluids)," International Journal of Heat and Mass Transfer, vol. 49, no. 1-2, pp. 240-250, Jan. 2006.

[8] X. Wang, and A. S. Mujumdar, "Heat transfer characteristics of nanofluids: a review," International Journal of Thermal Sciences, vol. 46, no. 1, pp. 1-19, Jan. 2007.

[9] S. K. Das, S. U. S. Choi, W. Yu, and T. Pradeep, *Nanofluids: Science and Technology*, New York, U.S.A.: Wiley, 2007.

[10] D. Singh, E. Timofeeva, W. Yu, J. Routbort, D. France, D. Smith, and J. M. Lopez-Cepero, "An investigation of silicon carbide-water nanofluid for heat transfer applications," Journal of Applied Physics, vol. 105, no. 6, pp. 064306, Mar. 2009.

[11] D. Wen, G. Lin, S. Vafaei, and K. Zhang, "Review of nanofluids for heat transfer applications," Particuology, vol. 7, no. 2, pp. 141-150, Apr. 2009.

[12] W. Yu, D. M. France, J. L. Routbort, and S. U. S. Choi, "Review and comparison of nanofluid thermal conductivity and heat transfer enhancements," Heat Transfer Engineering, vol. 29, no. 5, pp. 432-460, 2008.

[13] H. Chen, and Y. Ding, "Heat transfer and rheological behaviour of nanofluids - a review," Advances in Transport Phenomena, vol.1, L. Wang, Springer Berlin Heidelberg, 2009, pp. 135-177.

[14] A. Ghadimi, R. Saidur, and H. S. C. Metselaar, "A review of nanofluid stability properties and characterization in stationary conditions," International Journal of Heat and Mass Transfer, vol. 54, no. 17-18, pp. 4051-4068, Aug. 2011.

[15] V. Sridhara, and L. N. Satapathy, "Al_2O_3-based nanofluids: a review," Nanoscale Research Letters, vol. 6, no.1, pp. 456, Dec. 2011.

[16] J. M. Wu, and J. Zhao, "A review of nanofluid heat transfer and critical heat flux enhancement - Research gap to engineering application," Progress in Nuclear Energy, vol. 66, pp. 13-24, Jul. 2013.

[17] R. S. Vajjha, and D. K. Das, "Experimental determination of thermal conductivity of three nanofluids and development of new correlations," International Journal of Heat and Mass Transfer, vol. 52, no. 21-22, pp. 4675-4682, Oct. 2009.

[18] M. P. Beck, Y. Yuan, P. Warrier, and A. S. Teja, "The thermal conductivity of alumina nanofluids in water, ethylene glycol, and ethylene glycol + water mixtures," Journal of Nanoparticle Research, vol. 12, no. 4, pp. 1469-1477, May. 2010.

[19] B. LotfizadehDehkordi, S. N. Kazi, and M. Hamdi, "Viscosity of ethylene glycol + water based Al_2O_3 nanofluids with addition of SDBS dispersant," in Processing and Properties of Advanced Ceramics and Composites V: Ceramic Transactions, vol. 240, Hoboken, NJ: John Wiley & Sons, Inc., 2013, pp. 211-218.

[20] T. Yiamsawas, O. Mahian, A. S. Dalkilic, S. Kaewnai, and S. Wongwises, "Experimental studies on the viscosity of TiO_2 and Al_2O_3 nanoparticles suspended in a mixture of ethylene glycol and water for high temperature applications," Applied Energy, vol. 111, pp. 40-45, Nov. 2013.

[21] L. S. Sundar, E. V. Ramana, M. K. Singh, and A. C. M. Sousa, "Thermal conductivity and viscosity of stabilized ethylene glycol and water mixture Al_2O_3 nanofluids for heat transfer applications: an experimental study," International Communications in Heat and Mass Transfer, vol. 56, pp. 86-95, Aug. 2014.

[22] E. V. Timofeeva, "Nanofluids for heat transfer - potential and engineering strategies," in Two Phase Flow, Phase Change and Numerical Modelling, A. Ahsan, Croatia: InTech, 2011, pp. 435-450.

[23] J. Jung, H. Oh, and H. Kwak, "Forced convective heat transfer of nanofluids in microchannels," in Proceedings of ASME IMECE, Chicago, IL, 2006, pp. 327-332.

[24] D. P. Kulkarni, R. S. Vajjha, D. K. Das, and D. Oliva, "Application of aluminum oxide nanofluids in diesel electric generator as jacket water coolant," Applied Thermal Engineering, vol. 28, no. 14-15, pp. 1774-1781, Oct. 2008.

[25] R. S. Vajjha, D. K. Das, and P. K. Namburu, "Numerical study of fluid dynamic and heat transfer performance of Al_2O_3 and CuO nanofluids in the flat tubes of a radiator," International Journal of Heat and Fluid Flow, vol. 31, no. 4, pp. 613-621, Aug. 2010.

[26] S. M. Peyghambarzadeh, S. H. Hashemabadi, S. M. Hoseini, and M. Seifi Jamnani, "Experimental study of heat transfer enhancement using water/ethylene glycol based nanofluids as a new coolant for car radiators," International Communications in Heat and Mass Transfer, vol. 38, no. 9, pp. 1283-1290, Nov. 2011.

[27] W. Yu, H. Xie, Y. Li, L. Chen, and Q. Wang, "Experimental investigation on the heat transfer properties of Al_2O_3 nanofluids using the mixture of ethylene glycol and water as base fluid," Powder Technology, vol. 230, pp. 14-19, Nov. 2012.

[28] P. Selvakumar, and S. Suresh, "Thermal performance of ethylene glycol based nanofluids in an electronic heat sink," Journal of Nanoscience and Nanotechnology, vol. 14, no. 3, pp. 2325-2333, Mar. 2014.

[29] X. W. Zhu, Y. H. Fu, J. Q. Zhao, and L. Zhu, "Three-dimensional numerical study of the laminar flow and heat transfer in a wavy-finned heat sink filled with Al_2O_3/ethylene glycol-water nanofluid," Numerical Heat Transfer, Part A: Applications, vol. 69, no. 2, pp. 195-208, Jan. 2016.

[30] Beckman Coulter, Inc. (2008, Sep.). Delsa™Nano Submicron Particle Size and Zeta Potential, Particle Analyzer User's Manual. [Online]. Available: https://www.beckmancoulter.com

[31] A. Beer, "Determination of the absorption of red light in colored liquids," Annalen der Physik und Chemie, vol. 86, no. 5, pp. 78-88, 1852.

[32] P. Fritz, P. Selembo, R. Pellet, S. Yavuzkurt, and N. Vaidya, "Heat exchange characteristics of silicate and carboxylate-based coolants in air-cooled engine parts," SAE International, 2001-01-1185, Mar. 2001.
[33] K. Mollenhauer, and J. Eitel, "Engine cooling," in *Handbook of Diesel Engines*, 1st ed. Germany: Springer, 2010, pp. 291-338.

[34] Y. A. Çengel, *Heat and Mass Transfer: A Practical Approach*, 3rd ed. U.S.A.: McGraw-Hill, 2006.

[35] C. Monrad, and J. Pelton, "Heat transfer by convection in annular spaces," presented at the Joint Symposium with the Heat Transfer Division of ASME, Boston, MA, 1942, pp. 593-611.

[36] A. Foust, and G. Christian, "Non-boiling heat transfer coefficients in annuli," presented at the meeting of American Institute of Chemical Engineers, Buffalo, NY, 1940, pp. 541-554.

[37] F. Dittus, and L. Boelter, "Heat transfer in automobile radiators of the tubular type," in University of California Publications in Engineering, vol. 2. Berkeley, CA: University of California Press, 1930, pp. 443-461.

[38] E. S. Davis, "Heat transfer and pressure drop in annuli," Transactions of ASME, vol. 65, pp. 755-760, Oct. 1943.

[39] W. H. McAdams, *Heat Transmission*, 3rd ed. U.S.A.: McGraw-Hill, 1954.

[40] J. H. Wiegand, E. L. McMillen, and R. E. Larson, "Discussion on: annular heat transfer coefficients for turbulent flow," American Institute of Chemical Engineers, vol. 41, pp. 147-153, 1945.

[41] D. Liu, and L. Yu, "Single-phase thermal transport of nanofluids in a minichannel," Journal of Heat Transfer, vol. 133, no. 3, pp. 031009, Mar. 2011.

[42] R. Prasher, P. E. Phelan, and P. Bhattacharya, "Effect of aggregation kinetics on the thermal conductivity of nanoscale colloidal solutions (nanofluid)," Nano Letters, vol. 6, no. 7, pp. 1529-1534, Jul. 2006.

[43] S. Lee, S. U. S. Choi, S. Li, and J. A. Eastman, "Measuring thermal conductivity of fluids containing oxide nanoparticles," Journal of Heat Transfer, vol. 121, no. 2, pp. 280-289, May. 1999.

[44] S. K. Das, N. Putra, P. Thiesen, and W. Roetzel, "Temperature dependence of thermal conductivity enhancement for nanofluids," Journal of Heat Transfer, vol. 125, no. 4, pp. 567-574, Jul. 2003.

[45] J. A. Eastman, U. S. Choi, S. Li, L. J. Thompson, and S. Lee, "Enhanced thermal conductivity through the development of nanofluids," in Materials Research Society Proceedings, Boston, MA, 1996, vol. 457, pp. 3-12.

[46] L. Jiang, L. Gao, and J. Sun, "Production of aqueous colloidal dispersions of carbon nanotubes," Journal of Colloid and Interface Science, vol. 260, no. 1, pp. 89-94, Apr. 2003.

[47] Y. Hwang, J. K. Lee, C. H. Lee, Y. M. Jung, S. I. Cheong, C. G. Lee, B. C. Ku, and S. P. Jang, "Stability and thermal conductivity characteristics of nanofluids," Thermochimica Acta, vol. 455, no. 1-2, pp. 70-74, Apr. 2007.

[48] S. Jana, A. Salehi-Khojin, and W. H. Zhong, "Enhancement of fluid thermal conductivity by the addition of single and hybrid nano-additives," Thermochimica Acta, vol. 462, no. 1-2, pp. 45-55, Oct. 2007.